Title: Conserved neural dynamics and computations across species in olfaction

Authors: Doris Ling*[1], Elizabeth H Moss*[2], Cameron L Smith[3], Ryan Kroeger[3], Jacob Reimer[3], Baranidharan Raman[#1], Benjamin R Arenkiel[#2]

Affiliations:

[1] Department of Biomedical Engineering, Washington University in St. Louis, St. Louis, MO

[2] Department of Molecular and Human Genetics, Baylor College of Medicine, Houston, TX,

[3] Department of Neuroscience, Baylor College of Medicine, Houston TX.

*These authors contributed equally.

[#]Corresponding authors: barani@wustl.edu and arenkiel@bcm.edu

Abstract

Interpreting chemical information and translating it into ethologically relevant output is a common challenge of olfactory systems across species. Are computations performed by olfactory circuits conserved across species to overcome these common challenges? To understand this, we compared odor responses in the locust antennal lobe (AL) and mouse olfactory bulb (OB). We found that odors activated nearly mutually exclusive neural ensembles during stimulus presentation ('ON response') and after stimulus termination ('OFF response'). Strikingly, ON and OFF responses evoked by a single odor were anticorrelated with each other. 'Inverted' OFF responses enhanced contrast between odors experienced close together in time. Notably, OFF responses persisted long after odor termination in both AL and OB networks, indicating a form of short-term memory. Taken together, our results reveal key neurodynamic features underlying olfactory computations that are conserved across insect and mammalian olfactory systems.

Introduction

Olfactory systems across species have the common requirement of translating chemical information into neuronal activity that then drives appropriate behaviors. To achieve this, species ranging from aquatic invertebrates to terrestrial mammals employ neural circuits that have remarkable similarities in their overall layout or architecture[1,2]. However, olfactory sensory organs of vertebrate and invertebrate species sample chemical cues present in their environment differently. For example, insect olfaction relies on odor molecules making direct contact with external antennae, whereas mammalian olfaction requires respiration to internalize odor molecules to bring them into contact with the olfactory epithelium[2]. In addition, variations in signal detection mechanisms (e.g., sniffing vs antenna flicking) cause variations in how olfactory cues are sampled during an encounter. While both vertebrate and invertebrate systems use large families of seven-transmembrane proteins for sensing odors, in vertebrates they function as G-protein coupled receptors[3] whereas in insects they act as ligand-gated ion channels[4]. The resulting differences in the structure of sensory input cause markedly different temporal dynamics in odor inputs and odor-evoked neuronal activity[5–7]. In addition, early olfactory circuits of the invertebrate antennal lobe (AL) have been studied predominantly as feed-forward neural networks[8–10]. In comparison, their vertebrate counterparts in the olfactory bulb (OB) receive massive centrifugal feedback projections[11–14], suggesting that more complex processing begins at the first circuit node that receives chemosensory input.

Despite these differences, olfactory systems have common needs that are conserved across species. These include sensitivity and specificity across a complex chemical space, a broad dynamic range, the ability to filter and emphasize different inputs, and the capacity to distinguish distinct odors from complex backgrounds[15–22]. Are these common needs met by shared circuit mechanisms and computational principles across species? Or do different odor sampling methods and olfactory circuit architectures substantially change how odors are represented and processed by vertebrate and invertebrate systems? By comparing neural dynamics in early olfactory processing centers across

diverse species, we have identified shared computational principles for how odor information is represented and processed over time – particularly after an odor stimulus ends.

In many sensory circuits, not just olfaction, stimulus-specific information is encoded across space (as neuronal ensembles), and over time (in neural dynamics). Neural responses evoked by even a brief encounter with a stimulus often continue well after stimulus termination as sensory 'aftereffects'[23–26]. Such persistent neural activity after the cessation of the stimulus, if stimulus-specific, could provide a neural basis for short-term sensory memory. Whether a transient odor leaves behind a fingerprint ('afterimage'), and whether such activity provides a crucial computational building block that underlies the adaptive processing capabilities of olfactory circuits remains to be understood.

To address these questions, we compared population-level odor response dynamics across insect and mammals, with the goal of identifying conserved computational principles that guide olfaction. Using *in vivo* electrophysiology in the locust AL, and meso-scale two-photon calcium imaging of mitral and tufted cell responses in the mouse OB, we captured neuronal ensemble responses to passive odor presentations. First, we revealed highly conserved neural population dynamics to odor stimuli across locusts and mice, two species with markedly different olfactory system organization. More specifically, we found that the ensembles of neurons activated during odor presentations (ON response) are different from those that become responsive after stimulus termination (OFF response). This results in distinct categories of nearly mutually exclusive ON and OFF neuronal response patterns across odors. Strikingly, neuronal ensembles in both locust AL and mouse OB have responses to the onset and the offset of individual odors that are inverted relative to each other (i.e., ON and OFF population response vectors are anticorrelated). These similar neural dynamics across mouse and locust underly two emergent computations that are shared by both species: contrast enhancement and short-term olfactory memory. Intriguingly, such computations are critical for animals navigating in the world, following odor trails, encountering new odors within complex backgrounds, and sensing odors in temporally complex plumes. Together, our results suggest that several

fundamental building blocks of olfactory computations are conserved across insect and mammalian olfactory systems.

Results

OFF responses form anticorrelated odor afterimages across species

To assay population-level odor-evoked activity in the locust antennal lobe (AL), we recorded extracellular electrophysiological activity of AL projection neurons (PN) during passive odor presentations (**Fig. 1A-B**). Notably, the majority of responsive PNs during the odor presentation (ON responders) became silent after stimulus termination (**Fig. 1C**). Conversely, neurons that were suppressed during odor presentation became activated after stimulus termination (OFF responders). The mean spike counts across all ON and OFF responsive PNs (**Fig. 1C**, traces) revealed the mutually exclusive nature of responses in these two subsets of projection neurons.

Distinct odor-evoked ON and OFF responsive PN subsets indicated that the overall neural activity during the odor ON and OFF time periods would be highly dissimilar. To qualitatively visualize these neural responses and monitor how they evolved as a function of time, we used a response trajectory analysis. For this, we regarded spike counts in 50 ms time bins across all recorded neurons as a high dimensional vector. These high-dimensional neural response vectors were projected onto three dimensions that captured a large fraction of the data variance (**Fig. 1D**; Principal Component Analysis or PCA; n = 66 PNs). As can be expected from the odor response heatmaps, the neural response vectors during ON periods (orange trajectories; 4 s during the odor presentation) were distinct from the ensemble responses during OFF periods (blue trajectories; 4 s from the termination of odorant). Notably, the dissimilarity between the neural activity vectors observed during both the stimulus presentation and after termination, was maintained for the entire 4 s window used for this analysis.

Next, to quantitatively examine the dissimilarity between ensemble ON and OFF responses, we applied a correlation analysis using the high-dimensional response vectors. For this we calculated pairwise correlations between all PN response vectors observed at different time points as a correlation matrix (**Fig. 1E**). Each row or column of the correlation matrix indicates the similarity between an ensemble response vector at a specific time point with all other PN response vectors observed over time. Consistent with the observed neuronal activity and PCA trajectory analysis, neural responses over time within the ON period (for the duration of the odor presentation) were highly correlated amongst one another. This high ON vs. ON intra-period correlation is reflected by the yellow diagonal block at the center of the correlation matrix. Similarly, OFF responses were highly correlated with one another, as indicated by the second yellow diagonal block at the bottom right of the correlation matrix. However, the cross-correlation between any ON response vector with any OFF response vector was greatly reduced compared to intra-period correlations. The low inter-period, ON vs OFF correlations are reflected by the blue, off-diagonal patches in the correlation matrix. These results show that the measured ON and OFF neural response vectors were highly distinct from one another.

Finally, we examined whether the distributions of angles between ON and OFF response vectors (a measure of dissimilarity) were consistent across a panel of diverse odors. For each odor, we calculated the angle between the high-dimensional PN response vectors for timepoints during the odor presentation and after the odor presentation. Vector comparisons fell into three groups: (1) comparing vectors from the ON period to other vectors from the ON period (ON vs ON; 80 vectors, 3160 pairwise comparisons), (2) comparing vectors from the ON period to vectors from the OFF period (80 ON vs 80 OFF vectors; 6400 pairwise comparisons) and (3) comparing vectors from the OFF period to other vectors from the OFF period (OFF vs OFF; 80 vectors, 3160 pairwise comparisons). The distributions of angles were consistent across odors (**Fig. 1F**, **Fig. S1**). In contrast, angles between random vectors of the same dimensionality clustered with means and medians around 90° (gray distributions). To allow quantitative comparisons across odors, we computed the

median angular separation for each odor per category (**Fig. 1G**). For every odor the median angle between the ON and OFF responses was more than 90 degrees (mean = 106.7° +/- 0.84 SEM, n = 11 odors), reflecting the negative correlation between ON and OFF responses (**Fig. 1D**). These results are consistent with our prior results[27] and generalize our previous findings by showing that distinct neural ensembles are activated during and after presentations of a wide panel of odors – suggesting an odor specific afterimage that is distinct from the initial odor response.

Distinct odor ON and OFF responses have also been described in the mouse OB[24], but the specific relationship between ON and OFF responses is unknown. To test whether the differences between ON and OFF population response dynamics in the locust are also observed in the mouse, we performed a similar analysis of odor evoked responses recorded from the mouse OB. For this, we imaged glomerular-layer mitral and tufted cell dendrites in Thy1-GCaMP6f mice using a two-photon random access mesoscope[28] during passive odor presentations (**Fig. 2A**). Calcium signals from hundreds of glomeruli (median: 215 glomeruli per imaging session) across the dorsal surface of bilateral OBs were monitored with high spatial and temporal resolution (**Fig. 2B-C**).

We found that, like locust PNs, distinct sub-populations of mitral and tufted cells uniquely responded to odor onset or odor offset (**Fig. 2D**). These data are consistent with previous studies that showing that neural responses in the mouse olfactory bulb continue after termination of the stimulus[24]. Our data further showed that glomeruli responding to odors during their presentations tended to be suppressed following odor offset, and that glomeruli responding most strongly to odor offset were suppressed during the odor presentation (i.e., ON and OFF responses were mutually exclusive (**Fig. 2D**, traces). Dimensionality reduction by principal components showed that the temporal trajectories of both ON and OFF responses to single odor presentations were distinct (**Fig. 2E**). Intriguingly, the pairwise correlation of glomerular response vectors over time, across odor presentations, and after odor offset, revealed that odor ON and OFF responses were not just distinct, but were anticorrelated,

while, in contrast, angular separation between scrambled vectors clustered around 90° (**Fig. 2F**). Thus, odor ON and OFF responses in the mouse OB displayed a remarkably similar relationship to that observed in the locust (**Fig. 2 E, F** *vs.* **Fig. 1D, E**). In the high-dimensional feature space, the angle between ON and OFF trajectories was greater than 90° for each odor presented (mean = 121.8° +/- 2.98 SEM, n = 4 odors, 7 sessions) (**Fig. 2G, H**), revealing that, as in the locust, odor ON and OFF responses in mouse OB glomeruli are inverted relative to each other and not merely independent (orthogonal) responses. Together these data suggest that odor-evoked aftereffects in the mouse OB and locust AL form an inverted odor afterimage.

ON and OFF responses occupy distinct regions of feature space

Next, we examined the extent to which population odor responses were separable by odor identity during ON and OFF time periods. Towards this, we first reduced the dimensionality of the ON responses across odors for visualization (**Fig. S2A**). This analysis revealed that each ON response formed a distinct trajectory that pointed in a different direction, indicating that unique populations of PNs were activated during each odor's ON period. Similarly, the OFF responses across the odors also formed distinct trajectories (**Fig. S2B**). We then compared how odor-specific information contained during ON and OFF time periods was organized with respect to one another. For this purpose, we performed principal components including neural responses during both ON and OFF periods. Our results indicated that ON and OFF periods occupied different regions of PCA space. This suggests that ON responses for different odors were markedly more similar to each other than they were to OFF responses across odors (**Fig. 3A**). To quantitatively validate the observations from PCA analysis, we used high-dimensional response vectors to calculate angular separation between the ON response elicited by a reference odor with the ON and OFF responses elicited by all odors in the odor panel (Fig. 3B). We found that ON responses of the reference odor had smaller angular separation with ON response vectors of all other odors compared to the OFF response vector of the same reference odor, as well as OFF responses to other odors. This finding was consistent for 5 out of 11 odors in the panel (**Fig. S3A**).

To further evaluate this result, we next calculated the correlations between ON and OFF responses of all odors in the panel (**Fig. 3C**). As expected, the upper left and lower right diagonal blocks summarizing intra-period correlation values (ON vs. ON and OFF vs. OFF) showed relatively high correlations. In comparison, the inter-period comparisons (ON vs. OFF, upper right and lower left off-diagonal blocks) showed lower correlations. Hierarchical clustering of high dimensional ON and OFF responses revealed that PN responses during ON and OFF periods formed distinct response clusters (**Fig. 3D**). Similar to the locust data, we compared dimensionality-reduced mouse glomerular response trajectories across odors. Consistent with the locust results, we found that both ON and OFF responses were odor-specific (**Fig. S2C, D**), and that ON responses occupied a distinct region of PCA space compared to OFF responses (**Fig. 4A**). We then corroborated these qualitative observations by quantifying the angular separation between the ON and OFF vectors in full-dimensional space (**Fig. 4B**). As in locusts, angular separations between a reference odor and all other odor ON responses were smaller than angular separations between the reference ON response and all odor OFF responses. This result was true for all odors in the panel (**Fig. S3B**). Given this observation, we reasoned that if ON responses were distinct from OFF responses in general, we would expect that, across odors, ON responses would be more like other ON responses, whereas OFF responses would be more like other OFF responses. To test this, we correlated the mean glomerular response vectors during ON and OFF periods of different odor presentations (**Fig. 4C**). Additionally, distributions of correlations across odors revealed systematically lower correlations for inter-period compared to intra-period correlations in both mouse and locust (**Fig. S4**). Supporting this, hierarchical clustering cleanly separated ON and OFF responses (**Fig. 4D**), showing that, as in the locust AL (**Fig. 3D**), ON and OFF responses in the mouse OB represent distinct patterns of neuronal activity.

Contrast is enhanced between sequentially presented odors

Given that odors can be recognized within hundreds of milliseconds of stimulus onset[29], how can OFF responses, which begin after a stimulus has been terminated, contribute to odor processing? One intuitive possibility is that neural activity after stimulus offset could interfere with subsequent odor responses. To test this hypothesis, we presented locusts with pairs of odors in quick succession, such that the OFF response of the first odor would overlap with the ON response of the second odor in the sequence (**Fig. 5A**). In locusts, we found that PNs that selectively responded to only one odor in the sequence maintained those responses whether the odors were encountered solitarily or in a sequence (i.e., unique responses were unperturbed; **Fig. 5A**, PN 1 and 2). Whereas PNs that responded to both odors individually, responded only to the first odor when the two odors were presented in sequence (**Fig. 5A**, PN 3). The response to the second odor was suppressed (i.e., overlap reduction).

Given that individual PN responses evoked by an odorant depend on previously encountered stimuli, we expected AL ensemble activity to vary systematically as a function of prior odor exposure. To test this, we first visualized PN neural responses evoked by a single odorant (geraniol, ger) encountered by itself ("solitary") or as the second odor in a two-odor sequence ("sequential") (**Fig. 5B**). As expected, presentations of geraniol after other odors produced response trajectories that relied on the prior odor in the sequence. Comparing response trajectories evoked during the solitary and sequential geraniol presentations, we found that geraniol responses during the sequential encounters became more distinct (greater angular separation) with respect to the first odor in that sequence (blue trajectories in **Fig. 5C**). This was observed for each odor sequence tested. Consistent with the PCA trajectory analysis, we found that the correlation between high-dimensional odor response vectors was lower when the odors were sequentially presented, compared to when the odors were presented in isolation (**Fig. 5D, E**). Together, these data support the hypothesis that inverted OFF responses among locust PNs allow AL circuits to enhance response contrast between sequentially encountered odorants.

We next questioned if the observed OFF responses play a similar role in enhancing contrast between odor representations in the mouse OB. To test this directly, we presented mice with either solitary odors, or odors in sequence (**Fig. 6A**). As observed for locust PNs (**Fig. 5**), overlapping subsets of glomeruli responded to individual odors when presented solitarily. However, when those same odors were presented sequentially, the glomeruli that responded to the first odor were suppressed during the presentation of the second odor (**Fig. 6A**, traces). As in locust, suppressing overlapping glomerular activity caused response trajectories for the same odor to vary depending on stimulus history (**Fig. 6B**, **Fig. S5A**), and ensemble trajectories of sequentially presented odors reliably deflected away from the trajectory of a previously presented odor (**Fig. 6C**, **Fig. S5C**). This indicated that responses to odors became more distinct (i.e., decorrelated) during the sequential encounters. To quantify this history-dependent contrast enhancement, we computed correlations between high-dimensional odor response vectors when odors were presented solitarily and compared these values with the correlations between responses when the same odors were presented sequentially (**Fig. 6D**, **Fig. S5B**). The qualitative trajectory analyses, together with the high-dimensional correlation analyses showed that when odors were presented sequentially, responses in the mouse OB became less similar (**Fig. 6E**). Together, these results suggest that contrast enhancement by inverted odor OFF responses represent a computation of early olfactory circuitry that is conserved across locusts and mice.

Odor OFF responses persist as a form of short-term memory

The OFF response dynamics in locust AL and mouse OB represent persistence of odor-specific information after the termination of the stimulus, and therefore may be regarded as a form of short-term memory. This raised the question of how long, and in what form, odor information persists in olfactory neuronal networks. To examine this, we first observed how post-stimulus network activity in the AL and OB relates to odor-evoked responses. As shown in prior analyses, distinct subsets of locust AL PNs (**Fig. 1**) and mouse OB glomeruli (**Fig. 2**) respond to odor onset (ON responders) and odor offset (OFF responders). We found that the activity of ON responders continued to be

suppressed, and the activity of OFF responders was elevated for several seconds after stimulus offset in both locust AL (**Fig. 7A**, **S6A**) and mouse OB (**Fig. 7B**). Further, neuronal activity in the AL and OB maintained negative correlations with the odor-evoked ON responses for several tens of seconds after stimulus termination (Locusts – **Fig. 7C, S6B**, Mouse – **Fig. 7D, S6C**). This result suggests that although the overall neural activity after stimulus termination returns rapidly to pre-stimulus levels, network activity remains negatively correlated or inverted with respect to the odor-evoked response.

The persistence of stimulus-specific activity patterns (an odor afterimage) in the locust AL and mouse OB indicated that odor identity could be inferred based on the post-stimulus ensemble activity, well after stimulus offset. To test this, we next performed a dimensionality reduction analysis of locust PN responses up to 20 seconds after stimulus offset. We visualized post-stimulus neural activity following different odors and found that the post-stimulus activity during the inter-trial interval period clustered robustly by odor identity (**Fig. 7E**). A simple k-nearest neighbor classifier, using angular distances of the full-dimensional ITI data, allowed robust odor discrimination (**Fig. 7F**). This confirmed the interpretation from the PCA analysis and showed that ITI activity was indeed odor-specific. We observed a similar clustering of 55-second ITI activity from the mouse OB (**Fig. 7G**), which contributed to highly accurate classification of odors from ITI glomerular responses (**Fig. 7H**). Additionally, we repeated this classification analysis using one-minute bins of glomerular activity taken from a 15-minute window between blocks of different odors (inter-block interval, IBI, **Fig. S6D**). Our results indicate that, during the IBI, network activity ceased to contain odor-specific information. We observed no clustering of binned responses taken from the IBI, and classification accuracy was at roughly chance levels (**Fig. S6E**).

Complementing the time-averaged classification analysis spanning the entire ITI period, we also performed a bin-by-bin classification analysis (**Fig. 7I-K**). We found that among locust PNs, odor information decayed slowly across the ITI. Classifier accuracy decreased to ~60% across odors throughout the 20-second post stimulus ITI, but notably, accuracy did not fall to chance levels during

the entire ITI period (**Fig.7I**). In the mouse OB, the persistence of odor information was even more striking. We found that classifier accuracy remained high across odors for the duration of the 55-second ITI (**Fig.7J**). However, classifier accuracy was greatly decreased during the 15-minute IBI (**Fig.7K**). Collectively, these findings indicate that AL PNs and OB glomerular activity maintains information about an odor stimulus well after its termination, and this short-term memory takes the form of anticorrelated activity that persists in the network.

Discussion

The goal of this study was to identify common computational principles that may govern odor response dynamics at early stages of the olfactory system across species. For this purpose, we used population imaging and electrophysiological recordings to compare the temporal dynamics of odor-evoked responses in the mouse OB and the locust AL, respectively. First, we showed that responses to odor onset (ON responses) and odor offset (OFF responses) are distinct and anticorrelated. We then demonstrated that OFF responses interfere with subsequent odor presentations and enhance contrast between sequentially presented odors in both mouse and locust. Finally, we found that inverted OFF responses persist and maintain short-term odor memories over several seconds. Taken together, these data reveal the functional consequences of long-lasting, temporally complex odor-evoked activity, and how they generalize across species. Further, our findings support the notion that odor response dynamics are conserved across systems and serve a core function of early olfactory circuits – contrast enhancement – in both the locust AL and mouse OB.

The complementary sets of neurons activated during ON and OFF periods can also be regarded as encoding equivalent, but complementary information with regards to changing stimulus intensity (i.e., increment vs decrement). Antagonistic pairs of olfactory sensory neurons have been reported in invertebrate antennas to encode information about increasing and decreasing odor concentrations[30]. Our results show that similar encoding exists at the ensemble level of second-order neurons in the

locust AL and mouse OB. An advantage of encoding information using complementary sets of ON and OFF neurons, is that inverted OFF responses form odor-specific memory traces. In other words, the identity of the odorant just encountered can be easily deduced by inverting the ensemble-level OFF responses. Whether this is a generic strategy for retaining stimulus specific information in neuronal networks over time, and whether complementarity in the activated sets of neurons also forms the basis for other adaptive computations remains to be seen.

Persistently altered neural dynamics and distortions in perception after an encounter with a stimulus are known as aftereffects[23]. Aftereffects represent a ubiquitous feature of sensory systems across species and have well described perceptual and behavioral consequences in visual, auditory, and somatosensory systems. In the visual system, an example of an aftereffect is the inverted afterimage perceived after fixating on a static image[31]. Importantly, the perceptual distortions of aftereffects reveal computations performed by sensory circuits that are critical for stimulus detection and discrimination. Aftereffects across sensory modalities and species correspond to changes in neuronal activity with stimulus offset – either through neuronal adaptation that occurs during stimulus presentation, or through distinct stimulus offset-evoked responses[31–35]. In olfaction, aftereffects have been described in the form of distinct neural responses to the offset of odors in worms, insects, fish, and mammals[24,27,36–38]. In the mammalian olfactory system, previous studies have shown that odor-specific information briefly persists in the OB after stimulus offset[24]. In contrast, we found that patterns of glomerular activity persisted for the duration of the ITI, allowing odor identification for up to a minute after presentation. This discrepancy is likely due to the different statistical methods used to quantify ensemble glomerular activity. Our analysis implemented K-NN classification of odors from neuronal activity based on the angular similarity between population response vectors. As such, our results build on previous studies to suggest that odor memories, in the form of ‘after images’, are longer lasting than previously appreciated. More importantly, our current work reveals a specific form of persistent ensemble neural activity, anticorrelated to odor-evoked responses, which allows information about recently encountered odors to influence subsequent odor responses.

Given the distinct nature of odor OFF responses, and the surprising finding that odor specific activity persists for tens of seconds after odor offset, an intriguing question is what cellular and circuit mechanisms drive these effects, and are they fixed or flexible? In locusts, it has been shown that (1) odor offset-evoked activity is distinct from odor onset-evoked activity, and (2) that OFF responses are anticorrelated with ON responses through a combination of cell-intrinsic properties and local GABAergic circuit interactions[27]. Part of this inverted OFF response relies on adaptive changes in spike-thresholds of individual PNs, such that PNs responding highly to an odor have elevated spike thresholds and are less-likely to respond at odor offset. On the other hand, those suppressed by an odor have lowered spike-thresholds and are more likely to fire at odor offset. At the same time, interconnectivity of PNs with local inhibitory interneurons also contributes to enhancing the inverted OFF responses[39]. Our current results suggest that OFF responses in mice are analogous to OFF responses in insect models in both structure and functional consequences – OFF responses are inverted relative to ON responses, and they serve to enhance contrast between subsequent odor presentations. Mitral and tufted cells (MTCs) in mice are analogous to locust PNs and exhibit similar features of intrinsic adaptation[31,40]. MTCs are also highly interconnected with both local inhibitory granule cells and periglomerular interneurons[41], which have been shown to contribute to OFF responses in the locust AL[27]. Thus, similar cellular and circuit mechanisms may underlie the inversion of odor OFF responses in mouse and locust models.

In contrast to the locust, however, the mouse OB receives extensive feedback from the olfactory cortex, as well as top-down cholinergic and noradrenergic modulation[11,13,14,42–45]. It has been suggested that persistent odor OFF responses in the mouse are centrally maintained and communicated to the OB via centrifugal feedback[24]. Indeed, differences in circuit mechanisms maintaining OFF responses in mouse and locust may contribute to the notable difference we observed in the persistence of the off response between the two models. Another notable difference between mouse and locust odor responses was the degree of anticorrelation in the OFF responses

(Figs. 1 and 2). One possible explanation is that the lower temporal resolution of two-photon imaging combined with the slower kinetics of GCaMP (compared to electrophysiology) may smooth observed odor responses over time, contributing to higher correlations within the odor period and stronger anticorrelations between ON and OFF periods. However, if this were the case, we would expect that when responses were averaged across ON and OFF periods (as in Figs. 3 and 4), the difference in the magnitude of the anticorrelations between the locust electrophysiology and mouse imaging datasets would decrease. However, this is not the case comparing the ON-OFF correlations in Figure 3D to the ON-OFF correlations in Figure 4D. Another possible explanation is increased cortical feedback and top-down control in the mouse olfactory system actively drive the inverted OFF response and give rise to more strongly anticorrelated activity compared to the locust model. Nevertheless, despite these differences, the surprising degree of conservation between mouse and locust ON-OFF dynamics, even when observed via very different recording modalities, suggests that equivalent circuit mechanisms may be driving and maintaining odor OFF responses in mouse and locust. However, future work will be required to test these hypotheses directly.

Finally, determining the perceptual quality of odor evoked aftereffects and their consequences for olfactory processing has proven challenging. While the conservation of persistent and distinct odor aftereffects across species implies that they are a useful feature of olfactory processing, the role of odor aftereffects, their perceptual analogs, and their impact on behavior remain unclear. To understand how odor OFF responses drive behavior, it has been shown that OFF responses in locusts correspond to a behavioral measure of “unsensing”[27]. Additionally, locust behavioral experiments are also beginning to reveal how the spatiotemporal structure of odor responses relate to perception of odor features like valence. Specifically, a recent study used behavioral experiments in locust to demonstrate that population odor response trajectories for different odors clustered according to the innate and even learned valences of the odors[46]. While these data suggest that OFF responses are behaviorally meaningful, future work will be required to determine precisely how odor

perception in mice and insects is shaped by odor OFF responses and how these effects impact odor-guided behavior.

Acknowledgments:

We thank Dr. Fabrizio Gabbiani for feedback on the manuscript. We thank Pearl Olsen for insect care, and Evelyne Tantry and Elaine Le for mouse care. This research was supported by NSF (1724218, 2021795) and ONR (N00014-19-1-2049, N00014-21-1-2343) grants to B.R., NIH (K99DC019505) to EHM, the McNair Medical institute, NIH awards (NINDS R01NS078294), (NIDDK R01DK109934), and DOD (PR180451-PRMP) awards to B.R.A, and NIH awards (NINDS UF1NS111692) to BRA and JR. Further support was also provided by the Neuroconnectivity Core at Baylor College of Medicine, which is supported by IDDRC Grant P50 HD103555 from the NICHD.

Author contributions:

BRA and BR conceived the collaborative study. DL, EHM, BRA and BR designed the experiments/analyses. DL performed all the locust electrophysiology experiments and analyzed the data. EHM performed mouse imaging data collection and pre-processing of the calcium imaging data with technical assistance from JR. CS created and managed data processing pipelines for mouse imaging data. RK collected imaging data. DL and EHM generated the figures and wrote the paper, BRA, JR and BR revised the manuscript. All authors carefully read and approved the manuscript. BR and BRA supervised all aspects of the work.

Data availability: All data presented in this paper will be publicly available in Figshare after the publication of this work.

Code Availability: Custom code used to generate figures in this paper will be publicly available along with the datasets in Figshare after the publication of this work.

Methods

Mice

All experimental procedures were approved by the Baylor College of Medicine Institutional Animal Care and Use Committee. Thy1-GCamp6f (Jax laboratories #025393) mice were used for 2-photon imaging experiments. Mice were housed in a standard 12-hour light/dark cycle and had *ad libitum* access to food and water.

Cranial window surgery

Chronic cranial windows were created in mice by removing a 4 mm diameter section of skull over the OB and inserting a glass coverslip. Before surgery mice were treated with 5 mg/kg Meloxicam. Anesthesia was induced and maintained with isoflurane during the surgical procedure. After induction of anesthesia, the scalp was injected subcutaneously with 0.05 mL bupivacaine, then cleaned and removed over the OB and dorsal skull. A 0.0.16'' thick stainless-steel shim (McMaster-Carr, A370-974) was centered over the OB and attached to the exposed skull with dental cement (C&B Metabond). A 4 mm diameter piece of skull was removed by carefully drilling though the skull. A 4 mm glass coverslip (Warner instruments) was placed over the exposed brain and sealed in place with tissue adhesive (3M Vetbond). The sealed window was then stabilized with high-viscosity cyanoacrylate superglue (Loctite). After the glue fully cured, the coverslip was protected with a cap of Kwik-Cast silicone elastomer (World Precision Instruments) which was removed immediately before imaging.

Odor delivery to mice

All imaging was performed on head-fixed, awake mice on a running wheel. Mice were head fixed using a custom headplate[47] designed to attach to the stainless-steel shim implanted on the skull during the cranial window surgery. Mice were habituated to the head fixation and imaging setup for at least 30 minutes prior to testing each day. For odor delivery, a multi-channel olfactometer[48] was

placed 6 cm in front of the mouse. The olfactometer provided a constant stream of room air into which experimental odors were injected. Odors were mixed into the central airstream before delivery to the mouse by an eductor positioned at the output of the olfactometer. Odors for mouse imaging experiments were obtained from Sigma and included methyl salicylate (msc), allyl sulfide (als), acetophenone (ace), and eugenol (eug), diluted to 10% by volume in mineral oil. Odors were further diluted to ~1% of their initial concentration by injection into the central airstream (~8 L/min flow rate). Odor delivery was controlled and synchronized with imaging via custom LabVIEW software. The timing of odor onset and offset was verified with PID (Aurora Scientific) recordings made adjacent to the mouse nostril. For solitary odor presentation experiments, odors were delivered individually for 5 seconds via injection into the central air stream. Each odor was repeated 10 times in a block with a 55 seconds intertrial interval between presentations within a block and 15 minutes between blocks of different odors. For sequential presentation blocks, odors were presented in pairs such that the first odor was presented for 5 seconds followed by a 1 second gap and then 5 seconds of the second odor. Odor pairs were presented in blocks of 10 with 49 seconds between trials within a block and 15 minutes between blocks of different odor pairs. Odors were scavenged after delivery by a constant vacuum positioned 10 cm behind the mouse in line with the air stream of the olfactometer.

Two-photon imaging

Two-photon imaging was performed on a ThorLabs/Janelia 2P-RAM mesoscope[28]. The laser wavelength was set to 920 nm to image GCaMP6f signals. Imaging parameters were controlled with ScanImage software. To maximize frame rates in each imaging session, fields of view were defined for acquisition that included a single plane visualizing only the dorsal surface of bilateral OBs (1800 um long x ~600um –wide fields of view that were tiled to cover a total field of view that was 1800-2500 um wide). Images were acquired continuously throughout experiments (during odor presentations, intertrial, and inter-block intervals), with 5um/pixel resolution at the fastest possible frame rate allowed by the imaging parameters (15-18 Hz). After imaging, videos were motion and raster-corrected and glomerular ROIs were manually defined with custom software. Following definition of glomerular

ROIs, fluorescence traces were extracted from ROIs, imported to MATLAB, converted to dF/F, and median filtered to remove any persistent motion artifacts.

Locust electrophysiology

Post-fifth instar adult locusts (*Schistocerca americana*) were reared in a crowded colony with a 12 hour-12 hour light-dark cycle. Both male and female were used for electrophysiological experiments. First, the locusts were immobilized with both antennae intact. Then the primary olfactory region of their brain, the antennal lobe (AL), was exposed, desheathed, and perfused with room temperature saline. Extracellular multiunit recordings of projection neurons (PNs) were performed with a 16-channel, 4x4 silicon probe (NeuroNexus) that was superficially inserted in the AL. Prior to each experiment, all probes were electroplated with gold to achieve impedances in the range of 200 to 300 kΩ. The recordings were acquired with a custom 16-channel amplifier (Biology Electronics Ship; Caltech, Pasadena, CA). The signals were amplified with a 10k gain, bandpass filtered (0.3 to 6 kHz), and sampled at 15 kHz using a LabView data acquisition system. A visual demonstration of this protocol is available online[49].

Odor delivery to locusts

Odor stimuli were delivered using a standard protocol previously described in our earlier work[45]. The following odor panel was used for electrophysiological experiments: ammonia (amm), apple (app), benzaldehyde (bza), citral (cit), geraniol (ger), hexanol (hex), hexanoic acid (hxa), isoamyl acetate (iaa), 1-nonanal (nan), z-3-nonen-1-ol (nen), nonanoic acid (noa), octanoic acid (oca), octanol (oct), phenethylamine (phn), and 4-vinyl anisole (vny). All odors were diluted in mineral oil to 1% v/v concentration and sealed in 60mL glass bottles with an air inlet and outlet. A pneumatic picopump (WPI Inc., PV-820) was used to deliver 0.1L/min of air to the odor bottle. The injected air displaced air containing diluted odorant in the bottle headspace, which was subsequently mixed with a desiccated

0.75L/min carrier air stream directed towards the locust antennae. A vacuum funnel placed behind the locust preparation continuously removed delivered odors.

PN spike sorting

To obtain single-unit PN responses, spike sorted was performed offline using four recording channels and conservative statistical principles[50]. Spikes belong to single PNs were identified as described in earlier work[51]. The following criteria were used to identify single units: cluster separation > 5 x noise standard deviations, total number of spikes within 20 ms inter-spike interval < 6.5% of total spikes, and spike waveform variance < 6.5 x noise standard deviations. In total, 66 PNs from 15 locusts were identified for data shown in **Figs.1** and **3**; and 85PNs were identified from 9 locusts for data shown in **Figs**. **5** and **7**.

Summary of locust and mice datasets

Two locust datasets were used to generate **Fig.1, 3, 5**, and **7**. The dataset used for generating **Figs. 5** and **7** were part of an earlier published dataset[52]. Seven mouse datasets were used to generate **Fig. 2**, **4**, **6**, and **7**. All datasets are summarized in **Supplemental Table 1**.

Data analysis, and statistics.

Time-bin-by-time-bin correlation analysis

Each pixel or matrix element in time-bin-by-time-bin correlation plots (**Fig.1E**, **2F**, **7C**, **D**) indicates the correlation value between neural activity vectors observed in the ith and j^{th} time bins. All time-bin-by-time-bin correlation analyses were computed using high-dimensional response vectors. Correlations were calculated as:

$$C_{ij} = \frac{cov\left(X_i^{ON}, X_j^{OFF}\right)}{\sigma_i^{ON}\sigma_j^{OFF}} \quad \textit{(Equation 1)}$$

Here, X is a n-dimensional activity vector, *i* and *j* represent time bins, X_i^{ON} represents the population activity vector in the ith time bin during the ON period, X_j^{OFF} represents the population activity vector in

the ith time bin during the ON period, $\sigma_i^{ON}, \sigma_j^{OFF}$ are standard deviations of spiking activities during ON and OFF periods during the ith and j^{th} time bins respectively.

For locust data, PN spikes were binned in 50 ms non-overlapping time bins, and spike counts of different PNs were concatenated to obtain a n-dimensional population spike count vector (where n = 66 PNs for **Fig. 1E**; n = 85 PNs for **Fig. 7C**). For mouse data, dF/F values were taken to be a n-dimensional population glomerular activity vectors (where n=73 glomeruli for **Fig. 2F**; n = 318 glomeruli for **Fig. 7D**).

Time averaged correlations analysis

All time averaged correlation analyses were computed using high-dimensional response vectors. Correlations were calculated as:

$$C = \frac{cov(X^{ON}, X^{OFF})}{\sigma^{ON}\sigma^{OFF}} \quad \textit{(Equation 2)}$$

Here, X^{ON}, X^{OFF} are trial- and time-averaged high-dimensional activity vectors for the ON and OFF periods, respectively, respectively.

For locust data, PN spikes during the 4 s odor stimulation were summed and averaged across ten trials to obtain a n-dimensional population PN average spike count vector (where: n = 66 PNs **for Fig. 3C**; n = 85 PNs for **Fig. 5D**). For mouse data, dF/F values were averaged across the 10 trials, and then averaged across the frames for the 5 second odor stimulation duration to obtain a n-dimensional population glomerular activity vector (where n = 198 glomeruli for **Fig. 4C**; n = 153 glomeruli for **Fig. 6D**).

Visualization of response trajectories through PCA

To visualize high dimensional AL PN spike counts and OB glomerular dF/F signals, we used a linear principal component analysis. For locust data, the spike counts for each PN in 50 ms time bin during the 4 second stimulation window were averaged across trials and concatenated across PNs to

generate a *n*-dimensional vector (where *n* = 66 PNs for **Fig. 1D**). The high-dimensional PN spike count vector was projected onto the top three eigenvectors of the data covariance matrix.

For mouse data, dF/F values at each imaging frame (captured at 15-19 Hz) during the 5 second stimulation window were averaged across trials and concatenated across glomeruli to generate a n-dimensional vector (where n = 198 glomeruli for **Fig. 2E**). The high-dimensional glomerular response vector was projected onto the top three eigenvectors of the data covariance matrix.

Visualization of ITI and IBI neural activity vectors through PCA

To visualize high dimensional AL PN spike counts and OB glomerular dF/F signals during intertrial intervals (ITI) and inter-block intervals (IBI) we used a linear principal component analysis. For locust data, the ITI was defined as the 20 seconds immediately following the odor offset. The spike counts for each PN were averaged across the 20 second ITI period. The resulting n-dimensional PN spike count vector (where n = 85 PNs for **Fig. 7E**) was computed for each trial and visualized after PCA dimensionality reduction. The data points were colored based on the odor that preceded the ITI analysis window. For mouse data, the ITI was defined as the 50 seconds immediately following the odor offset. The dF/F values were averaged across the 50 second ITI period for each glomerulus and the resulting n-dimensional glomerular activity vector (where n = 318 glomeruli for **Fig. 7G**) represented the glomerular activity following the odor offset for a given trial. Glomerular activity following odor termination in different trials were visualized after PCA dimensionality reduction, and the data points colored based on the odor that preceded the ITI period.

For mouse data, the IBI was defined as the 15-minute non-odor stimulation period between blocks of odor stimulation. The dF/F values were binned into 1-minute non-overlapping time bins across the 15-minute IBI period and concatenated. The resulting n-dimensional glomerular activity vector (where n = 318 glomeruli for **Fig. S6D**) represented the glomerular activity during the entire IBI period. The IBI activity vectors were visualized after dimensionality reduction and the data points colored based on the odor that was presented in the block of trials that preceded the IBI window.

Distribution of angles between high-dimensional response vectors

Vector angles were calculated between trial-averaged PN activity for each 50 ms time bin in the 4 second ON period (**Fig. 1F**, **2G**). The resulting vector angles were subsequently binned according to the ON-ON, ON-OFF, or OFF-OFF period depending on the time window from which the PN vectors were picked. A similar analysis was carried out for mouse OB glomerular responses using dF/F values from each imaging frame. As a control, the vector angles were calculated from high-dimensional normally distributed random vectors.

For hierarchical clustering, we first calculated the summed spike counts during 4 second odor presentations for each individual PN and generated a single vector (n = 66 PNs) for each odor. Similarly, dF/F values for each glomerular ROI in the mouse OB imaging datasets were averaged across the duration of an odor ON or OFF period. Dendrograms were generated using the angular distance between respective average odor responses. The cluster tree was created in such a way that the furthest pairwise distance between any two samples assigned to an individual cluster was minimized.

Classification analysis of average ITI periods

To classify ITI periods, we used a k-Nearest Neighbor (k-NN) classification algorithm.

For locust data, the ITI was defined as the 20 seconds immediately following the odor offset. The spike counts for each PN were binned in 50 ms non-overlapping time bins and averaged across the 20 second ITI period. The resulting n-dimensional PN spike count vector (where n = 85 PNs for **Fig. 7F**) represented the PN activity following the odor offset for a given trial. Then the PN spike count vectors were concatenated across the 10 trials and 7 odors, resulting in 70 trials for classification. The angular distance of the resulting high-dimensional PN spike count matrix was used as a distance measure and the most represented odorant amongst the 10 nearest neighbors was the label assigned to each trial (i.e., 10-nearest neighbor approach; leave-one-trial-out-validation).

For mouse data, the ITI was defined as the 50 seconds immediately following the odor offset. The dF/F values were averaged across the 50 second ITI period for each glomerulus and the resulting n-dimensional glomerular activity vector (where n = 318 glomeruli for **Fig. 7H**) represented the glomerular activity following the odor offset for a given trial. Then the glomerular activity vectors were concatenated across the 10 trials and 4 odors, resulting in 40 trials for classification (leave-one-trial-out validation). The angular distance of the resulting high-dimensional glomerular activity matrix was used to classify each trial based on the most represented odorant amongst the 50 nearest neighbors (i.e., 50 nearest neighbors). A larger *k*-value was used compared to the *k*-value used for locust ITI classification to account for the slower calcium indicator dynamics.

Classification analysis of average IBI periods

To classify IBI periods, we used a similar k-Nearest Neighbor (k-NN) classification algorithm.
For mouse data, the IBI was defined as the 15-minute non-odor stimulation period between blocks of odor stimulation. The dF/F values were averaged over 1-minute non-overlapping time bins across the 15-minute IBI period, resulting in n-dimensional glomerular activity vector (where n = 318 glomeruli for **Fig. S6D**). Then the glomerular activity vectors were concatenated across the 4 odors, resulting in 60 trials for classification (leave-one-trial-out cross-validation; *50-nearest neighbor approach*).

Time bin by time bin ITI classification analysis

For locust data, the ITI was defined as the 20 seconds immediately following the odor offset. The spike counts for each PN were binned in 50 ms non-overlapping time bins and averaged across the 10 trials. The resulting n-dimensional PN spike count vector (where n = 85 PNs **for Fig. 7I**) represented the trial-averaged PN activity following the odor offset. Then the PN spike count vectors were concatenated across the 7 odors, resulting in 2,800 time bins for classification. The angular distance of the resulting high-dimensional PN spike count matrix was used to classify each time bin

was assigned an odor label based on the nearest *k* points (where *k* = 10; leave-one-time-bin-out validation).

For mouse data, the ITI was defined as the 50 seconds immediately following the odor offset. The dF/F values were averaged across the 10 trials for each glomerulus and the resulting n-dimensional glomerular activity vector (where n = 318 glomeruli for **Fig. 7J**) represented the trial-averaged glomerular activity following the odor offset. Then the glomerular activity vectors were concatenated across the 4 odors, resulting in approximately 4,000 time-bins for classification. The angular distance of the resulting high-dimensional glomerular activity matrix was used to classify each element as the most common label of the nearest *k* points (where *k* = 50).

Time bin by time bin IBI classification analysis

To classify IBI periods, we used a k-Nearest Neighbor (k-NN) classification algorithm.

For mouse data, the IBI was defined as the 15 minute non-odor stimulation period between blocks of odor stimulation. The dF/F values per imaging frame during the 15 minute IBI period were calculated and the resulting n-dimensional glomerular activity vector (where n = 318 glomeruli for **Fig. 7K**) represented the glomerular activity during the entire IBI period. Then the glomerular activity vectors were concatenated across the 4 odors, resulting in 72,000 time bins for classification. The angular distance of the resulting high-dimensional glomerular activity matrix was used to classify each element as the most common label of the nearest *k* points (where *k* = 50).

Figure Legends

Fig. 1: Odor ON and OFF responses in the locust antenna lobe are anticorrelated.

A. Schematic of the experimental design. (top) Multi-unit extracellular electrophysiological signals were recorded from the projection neurons (PN) in the locust antennal lobe (AL). (bottom) Odors were presented to locusts in blocks of ten trials where a single odorant was repeatedly presented in all the trials within a block. Each trial was 1 minute in duration, and the odorant was presented for 4 seconds. A 15-minute gap separated two different blocks of trials. **B.** Representative trial-averaged PSTH traces of 24 PNs in response to benzaldehyde (bza), 4-vinyl anisole (vny), octanol (oct), and z-3-nonen-1-ol (nen). **C.** (top) PSTH traces from three ON-responding (orange, thin lines) and OFF-responding (thin blue lines) PNs are shown along with their means (thick lines). Note that during odor presentation, ON responders show responses that are above the pre-stimulus baseline levels, whereas the OFF responders are suppressed such that the responses are below the pre-stimulus activity levels. This trend is reversed after stimulus termination. (bottom) Trial-averaged odor-evoked responses of 66 PNs to z-3-nonen-1-ol (nen) over time are shown. PNs are sorted such that the ON responders are at the top and the OFF responders are at the bottom. Note that the overall trend of OFF responses being an inversion of ON activity. **D.** Representative dimensionality reduced temporal trajectories (thick lines) of trial-averaged PN activity during the 4-sec ON period of nen exposure (orange) and 4-sec OFF period (blue) are shown. Each point along the trajectory indicates population PN activity in a single 50-ms time bin. Spokes (thin lines) represent 200 ms time intervals. Open circles mark one second intervals along the trajectory. **E.** Representative temporal correlation of trial-averaged PN activity is shown. Each pixel represents the correlation between 66-dimensional PN response vectors in two different time bins. Correlation between PN activity vectors recorded before, during and after odor presentations are summarized in this plot. **F.** The distribution of angular separation between high-dimensional PN population vectors are shown. Three different pairwise comparisons are made between response vectors: between any two ON response vectors (orange), between any two OFF response vectors (blue), and between each ON response vector with every OFF response vector (yellow). Angular separation between 66-dimensional random vectors (grey) are

shown as a control distribution (with a mean and median around 90°). Distributions of angular separation are shown for four representative odors (vny, bza, oct, and nen). Median values of ON vs OFF period angular separation distributions are indicated using dashed lines and values listed using grey text. **G.** Summary of the median angular separation distribution for all 11 odors showing ON vs ON period median angles (orange), OFF vs OFF period median angles (blue) and ON vs OFF period median angles (yellow). Points corresponding to different odors are offset along the radius for visualization. The mean ON vs OFF angular distance observed across odorants is indicated using a dashed grey line.

Fig. 2: Odor ON and OFF responses in the mouse olfactory bulb are anticorrelated. **A.** Schematic of the experimental design. Awake mice were head fixed on a running wheel and presented with odors. A meso-scale two-photon microscope was used to image glomerular activity in the olfactory bulb. Closely matching the experimental structure in locusts, odors were presented in blocks of ten trials. Each odor exposure to mice was for 5 seconds with 55 seconds between consecutive trials. A 15-minute period of no odor stimulation separated blocks of different odors. **B.** Representative trial-averaged image of GCaMP fluorescence in the olfactory bulb of a Thy1-GCaMP6f mouse (left) shown with ROIs overlaid on glomeruli (right) from bilateral olfactory bulbs. Scale bar is 500 um. **C.** Fluorescence traces (dF/F) from 25 representative glomeruli are shown. The activity before, during, and after presentation in these 25 glomeruli are shown in response to acetophenone (ace, purple), methyl salicylate (msc, yellow), eugenol (eug, orange), and allyl sulfide (als, pink). **D.** (top) Average fluorescence (dF/F) trace from ON (orange) and OFF (blue) responsive glomeruli. Subsets of glomeruli were selected depending on whether they had stronger ON or OFF responses and their dF/F fluorescence traces are shown as a function of time. Notably, when ON responses were high, the dF/F in OFF responsive glomeruli were suppressed and *vice versa*. Hence, ON and OFF responses can be regarded as inversions of one another. (Bottom) Heatmap showing trial-averaged dF/F traces from all glomeruli in one mouse in response to allyl sulfide (als, pink bar) and after odor offset. **E.** Dimensionality reduced temporal trajectories of the trial averaged glomerular

population response during allyl sulfide presentation (als ON, orange) and after allyl sulfide presentation (als OFF, blue) are shown. **F.** Representative correlation matrix summarizing the similarity between trial-averaged glomerular responses evoked by allyl sulfide (als, pink bar) during both odor ON and OFF time periods is shown. Each pixel represents the correlation between glomerular response vectors observed at two timepoints. **G.** Distribution of angular distance between pairs of glomerular population response vectors are shown. Comparisons are made between pairs of glomerular response vectors during the ON period (orange), OFF period (blue), and between the ON and OFF period (yellow). Angular distance between randomized high-dimensional vectors of matching dimensions (grey) are shown as a control (mean and median around 90°). Angular distance distributions are shown for all four odors presented (ace, msc, eug, als). Median values of ON vs OFF response vectors angular distances are shown as grey text and dashed lines. **H.** Summary of the median angular distances for 4 odors (n = 7 imaging sessions from 4 mice) showing ON vs ON period median angles (orange), OFF vs OFF period median angles (blue) and ON vs OFF period median angles (yellow). The mean of the ON vs OFF angles is shown as the dashed grey line and grey text. Radii indicate different imaging sessions (n = 7 imaging sessions from = 4 mice).

Fig. 3: ON and OFF responses in locust antenna lobe contain distinct odor specific information. **A.** Dimensionality-reduced odor-evoked ON (orange) and OFF (blue) response trajectories for all 11 odors in the panel are shown. **B.** A polar plot of the angular distances between the hex ON response vector (reference, solid orange circle; averaged over 4 seconds odor presentation time window) and the ON response vectors of the 10 other odors (orange open circles) is shown. For comparison, the angular distances between the hex ON response vector and the OFF responses of all odors (blue open circles) including hex OFF response (solid blue circle) are shown. Arcs **(**thick lines) show the range of angular distances observed for ON-ON angular distances and compares the same with ON-OFF angular distances (note that all distances computed with respect to hex ON response vector). **C.** Correlation of trial-averaged PN ON and OFF responses to all eleven odorants in the panel. The higher the correlation (yellow) the greater the similarity between the two

response vectors. Note that all ON response vectors tend to be similar to each other. Similar trend also observed with OFF response vectors with respect to other OFF response vectors. Lower correlation values for ON-OFF vector comparisons indicate dissimilarity between these vectors (blue). **D.** Hierarchical clustering of ensemble PN ON and OFF responses are shown. Note that the data split into distinct ON (red) and OFF (blue) response clusters.

Fig. 4: ON and OFF responses in the mouse olfactory bulb contain distinct odor specific information. **A.** Dimensionality-reduced odor-evoked ON (orange) and OFF (blue) response trajectories of four odors: ace, msc, eug and als are shown. **B.** A polar plot showing the angular distance between the ace ON response vector (reference, solid orange circles) and either the ON response vectors of the 3 other odors (open orange circles), ace OFF response vector (solid blue circle), or OFF response vector of the three other odors (open blue circles). Different radii indicate responses from different imaging sessions (n = 7 imaging sessions from 4 mice). Arced lines show the range of angular distances between ON responses (orange). For comparison the range of angular distances between the ace ON response vector with OFF response vectors of all odorants (blue open circles) including ace OFF response vector (solid blue circle). **C.** Correlation matrix summarizing the similarity between glomerular ON and OFF responses evoked by four odors is shown. Glomerular response vectors were averaged across trials and over five second odor presentation windows (ON) or during the five seconds after odor offset (OFF). **D.** Hierarchical clustering of glomerular ON and OFF response vectors from one representative imaging session is shown. Consistent with the locust results, ON and OFF response vectors group into distinct clusters.

Fig. 5: Contrast is enhanced in the locust antenna lobe between odors presented sequentially. **A.** (top) Experimental design for sequential blocks. Odors presented include geraniol (ger), isoamyl acetate (iaa), benzaldehyde (bza), citral (cit), octanol (oct), and apple (app). 4 second pulses of Odor A were presented with 4 second pulses of Odor B presented 0.5 second afterwards during the OFF period of Odor A. (bottom) Example responses of two projection neurons (PN) to oct (left) and ger

(middle) presented individually and to ger presented in sequence with oct (right). PN1 responds to oct but not ger individually or in sequence. PN 2 responds to ger but not oct individually or in sequence. PN 3 responds to oct and ger individually, but the response to ger is suppressed when ger is presented in sequence with oct. **B.** Dimensionality reduced ON responses to ger. Each trace represents the average PN response during the ON period to ger in solitary (ger), or ger with different odors that presented immediately before ger (sequential: (app)ger, (bza)ger, (cit)ger, (iaa)ger, (oct)ger). **C.** (left) Dimensionality reduced ON responses to solitary iaa (blue), solitary ger (red), and ger sequentially after iaa ((iaa)ger, orange). (middle) Dimensionality reduced ON responses to solitary app (blue), solitary ger (red), and ger sequentially after app ((app)ger, orange). (right) Dimensionality reduced ON responses to solitary oct (blue), solitary ger (red), and ger sequentially after oct ((oct)ger, orange). **D.** Correlation of average PN ON responses to solitary odors (app, bza, cit, iaa, oct, ger) and to ger presented in sequence after other odors ((app)ger, (bza)ger, (cit)ger, (iaa)ger, (oct)ger). Each box represents the correlation between PN responses averaged over time and across trials for two different odor presentation conditions. White boxes and arrows indicate which correlation values are used for the quantitative comparison in (E). To the left of the arrows, the boxes highlight correlations between solitary presentations of ger with solitary presentations of other odors (solitary odor vs. solitary ger). To the right of the arrows, the boxes highlight correlations between presentations of ger in sequence with the other odor and solitary presentations of the other odors (solitary odor vs. sequential (odor)ger). **E.** Correlation values of PN population responses to solitary ger vs PN population responses to other solitary odors (left boxes in D) compared to correlation values of PN responses to solitary odors vs PN responses to ger presented sequentially after the other odors (right boxes in D, one-tailed t test, $p < 0.05$, $n = 5$ odor pairs).

Fig. 6: Contrast is enhanced in the mouse olfactory bulb between odors presented sequentially. **A.** (top) Schematic of odor presentations showing solitary presentations of single odors and sequential presentations of two odors with a one second interval between paired odors in a trial. Odors presented include acetophenone (ace), methyl salicylate (msc), eugenol (eug), and allyl sulfide

(als). 5 second pulses of Odor A were presented with 5 second pulses of Odor B presented 1 second afterwards during the OFF period of Odor A. (bottom) Example responses of three glomeruli (G) to ace (left) and msc (middle) presented individually and to msc presented one second after ace (right). G1 responds to ace and msc individually, but the response to msc is suppressed when ace is presented immediately before msc. G2 responds to ace but not msc individually or in sequence. G3 responds to msc but not ace individually or in sequence. **B.** Representative dimensionality reduced temporal trajectories showing the response to a solitary presentation of msc (dark red) and responses to msc sequentially presented after ace ((ace)msc), eug ((eug)msc), and als ((als)msc, lighter reds). **C.** Representative dimensionality reduced temporal trajectories showing responses to solitary and sequential presentations of msc. (left) Dimensionality reduced ON responses to solitary eug (blue), solitary msc (red), and msc sequentially presented after eug ((eug)msc, orange). (middle) Dimensionality reduced ON responses to solitary als (blue), solitary msc (red), and msc sequentially presented after als ((als)msc, orange). (right) Dimensionality reduced ON responses to solitary ace (blue), solitary msc (red), and msc sequentially presented after ace ((ace)msc, orange). **D.** Correlation of average glomerular responses during ON periods across solitary presentations of eug, ace, msc, and als as well as sequential presentations of msc following ace ((ace)msc), eug ((eug)msc), and als ((als)msc). Each box represents the correlation of trial averaged glomerular response vectors between odor presentation conditions from a representative imaging session. White boxes and arrows indicate which correlation values from the representative imaging session are used for the quantitative comparison in (E, left). To the left of the arrows, boxes highlight correlations between solitary presentations of msc with solitary presentations of other odors (solitary odor vs. solitary msc). To the right of the arrows, boxes highlight correlations between presentations of msc in sequence with other odors and solitary presentations of the other odors (solitary odor vs. sequential (odor)msc). **E.** (left) Correlation values between solitary presentations of msc and other odors (left boxes in D) compared to correlation values between sequential msc and odors across imaging sessions (right boxes in D, $n = 3$ imaging sessions from 2 mice; one-tailed t test, $p < 0.01$) (right). Correlation values between solitary presentations of ace and the three other odors (see also Figure

S5) compared to correlation values between sequential ace and odors across imaging sessions (n = 4 imaging sessions from 2 mice; one-tailed t test, $p < 0.05$).

Fig. 7: OFF responses maintain an odor-specific short-term memory in mouse OB and locust AL. **A.** Trial averaged PSTH traces from representative ON (thin orange) and OFF responsive (thin blue) PNs responsive to apple (app), citral (cit), or isoamyl acetate (iaa) are shown. Means of representative PNs are shown as thick lines. **B.** Trial averaged dF/F traces from representative ON (thin orange) and OFF (thin blue) responsive glomeruli in mouse OB showing pre odor, odor-evoked, and post-odor activity for methyl salicylate (msc), acetophenone (ace), allyl sulfide (als), and eugenol (eug). Mean dF/F of ON (thick orange) and OFF responders (thick blue) are shown. **C.** Representative temporal correlations of PN responses to app, cit, and iaa. Each pixel represents the correlation of the trial-averaged high-dimensional PN population response vectors between two 50 ms time bins. **D.** Representative temporal correlations of OB glomerular responses to ace and msc. Each pixel represents the correlation of the trial-averaged glomerular population response vector between two 63 ms time bins. **E.** Dimensionality-reduced ensemble PN activity during the 20 seconds immediately following odor offset are shown (i.e., during intertrial intervals (ITI) between presentations of the same odor within a block of 10 trials). Ten points of the same color represents the PN ensemble activity after the termination of the same odorant. **F.** Results from a K-NN classification analysis of PN activity are shown. Odor label was assigned based on ten nearest neighbors and angular separation using full-dimensional data was used as the distance metric. Note that only the PN activity during ITI period was used for this analysis. The overall classification rate was 97.1%. **G.** Dimensionality-reduced mouse OB glomerular activity during the 55 second ITIs between presentations of the same odor within a block of 10 trials. Each point represents population-level glomerular activity following the termination of the same odorant within a block of trials. **H.** Results from a K-NN classification analysis of the glomerular activity (k = 50) during the 55 second ITI period, based on angular distance using full-dimensional data, are shown. The classification rate of the glomerular ITI activity was 95%. **I.** (top) Time-bin-by-time-bin k-NN classifier (k = 10; angular distance

metric; locusts PN activities) predictions for the post stimulus ITI time bins are shown. Odor predictions at each timepoint are shown using a colors code. (bottom) Quantification of classifier accuracy during the ITI time window for each odor (colored transparent lines) and averaged across odors (black line) are shown. The chance-level is identified using the dashed grey line. **J.** (top) Time-bin-by-time-bin k-NN classifier (k = 50; angular distance; mouse glomerular activities) predictions of the post stimulus ITI time bins are shown. Odor predictions at each timepoint are again shown using color code. (bottom) Quantification of classifier accuracy during the ITI time window (colored transparent lines) and averaged across odors (black line) are shown. The chance level is again identified as the dashed grey line. **K.** (top) Time-bin-by-time-bin k-NN classifier (k = 50; mouse glomerular activities) predictions of the IBI time bins is shown. Odor predictions at each timepoint are identified using the same color code as in **panel J**. (bottom) Quantification of classifier accuracy for the IBI following each odor (colored transparent lines) and averaged across odors (black line).

Supplementary Figures:

Fig. S1: Distribution of angular shifts of PN population responses for remaining odors. Angular shifts in PN population responses comparing each time bin with every other time bin, showing results as probability density (radii) for remaining seven odors not shown in Fig.1. Odors include hexanol (hex), isoamyl acetate (iaa), 1-nonanal (nan), hexanoic acid (hxa), phenethylamine (phn), ammonia (amm), and nonanoic acid (noa). ON period time bins are compared to other ON period time bins (orange) and OFF-period time bins are compared to other OFF period time bins (blue) to show the spread of PN population responses within ON and OFF periods. ON period time bins are compared to OFF period time bins (yellow) to show the angular shift between ON and OFF responses. Points from random vectors (grey) are compared to show the centering of the random distributions around 90°. Median values of ON vs. OFF period angular distributions are shown as black text.

Fig. S2: Odor ON and OFF response trajectories projected onto separate principal components for locust and mouse. **A.** Dimensionality-reduced odor-evoked ON responses from the population of locust AL PNs. ON Responses to 8 odors are projected onto the top three principal component axes calculated using only the ON responses. Odors shown include benzaldehyde (bza), hexanoic acid (hxa), hexanol (hex), isoamyl acetate (iaa), 1-nonanal (nan), z-3-nonen-1-ol (nen), octanoic acid (oca), 4-vinyl anisole (vny). **B.** Dimensionality-reduced OFF responses from the population of locust AL PNs. OFF Responses to 8 odors are projected onto the top three principal component axes calculated using only the OFF responses. **C.** Dimensionality-reduced odor-evoked ON responses from a representative imaging session of mouse OB glomeruli. ON Responses to 4 odors are projected onto the top three principal component axes calculated using only the ON responses. Odors presented include methyl salicylate (msc), acetophenone (ace), eugenol (eug), and allyl sulfide (als). **D.** Dimensionality-reduced OFF responses from a representative imaging session of mouse OB glomeruli. OFF responses to 4 odors are projected onto the top three principal component axes calculated using only the OFF responses.

Fig. S3: Separation between ON and OFF responses across reference odors. **A.** Polar plots showing the median angle between the locust AL PN response vector for a reference odor (black text) ON response (solid orange circles), ON responses to the 10 other odors (open orange circles), the reference odor OFF response (solid blue circle), and OFF-responses to the 10 other odors (open blue circles). Quantification of angular shifts is shown for 10 reference odors not shown in Figure 3. **B.** Polar plots showing the median angle between the mouse OB glomerular response vector for a reference odor (black text) ON response (solid orange circles), ON responses to the 3 other odors (open orange circles), the reference odor OFF response (solid blue circle), and OFF responses to the 3 other odors (open blue circles). Quantification of angular shifts is shown for 3 reference odors not shown in Figure 3. Radii indicate different imaging sessions (N = 7 sessions from 4 mice).

Fig. S4: Distributions of correlation values across odor ON and OFF periods in mouse and locust. A. From locust data, histograms revealing probability density functions of correlation values comparing ON responses across odors (ON-ON, orange), OFF responses across odors (OFF-OFF, blue), and ON responses across odors to OFF responses across odors (ON-OFF, yellow). Solid line and shaded Gaussian distributions are maximum-likelihood fits of the three correlation distributions. **B.** From mouse data, histograms of correlation values comparing ON responses across odors (ON-ON, orange), OFF responses across odors (OFF-OFF, blue), and ON responses across odors to OFF responses across odors (ON-OFF, yellow). Gaussian distribution fit using maximum likelihood estimation is also shown.

Fig. S5: Contrast enhancement in the mouse olfactory bulb generalizes across odors. A. Representative dimensionality reduced temporal trajectories showing the response to a solitary presentation of acetophenone (ace, dark red) and responses to ace sequentially presented after methyl salicylate ((msc)ace), eugenol ((eug)ace), and allylsulfide ((als)ace, lighter reds). **B.** Correlation of average glomerular responses during ON periods across solitary presentations of eug, ace, msc, and als as well as sequential presentations of ace following msc ((ace)msc), eug ((eug)ace), and allyl sulfide ((als)ace). Each box represents the correlation of trial averaged glomerular response vectors between odor presentation conditions from a representative imaging session. White boxes and arrows indicate which correlation values from the representative imaging session are used for the quantitative comparison in Figure 6E. To the left of the arrows, boxes highlight correlations between solitary presentations of ace with solitary presentations of other odors (solitary odor vs. solitary ace). To the right of the arrows, boxes highlight correlations between presentations of ace in sequence with other odors and solitary presentations of the other odors (solitary odor vs. sequential (odor)ace). **C.** Representative dimensionality reduced temporal trajectories showing responses to solitary and sequential presentations of ace. (left) Dimensionality reduced ON responses to solitary eug (blue), solitary ace (red), and ace sequentially presented after eug ((eug)ace, orange). (middle) Dimensionality reduced ON responses to solitary als (blue), solitary

ace (red), and ace sequentially presented after als ((als)ace, orange). (right) Dimensionality reduced ON responses to solitary msc (blue), solitary ace (red), and ace sequentially presented after msc ((msc)ace, orange).

Fig. S6: OFF response persistence across odors through intertrial and inter-block intervals. A. Trial averaged PSTH traces from representative ON and OFF responsive ONs showing pre-odor, odor-evoked, and post odor activity for odors hexanol (hex), benzaldehyde (bza), geraniol (ger), and octanol (oct) reflecting the remaining odors not shown in Figure 7. **B.** Representative temporal correlations of PN responses to app, cit, ger, and oct, reflecting the remaining odors not shown in Figure 7. Each pixel represents the correlation of the trial averaged PN population response vectors between two 50 ms time bins. **C.** Representative temporal correlations of OB glomerular responses to eug and als. Each pixel represents the correlation of the trial averaged glomerular population response vector at one time point compared to one other time point. **D.** Dimensionality-reduced mouse OB glomerular responses during the 55-second intertrial intervals (ITIs, solid circles) and 15-minute inter-block intervals (IBIs, open circles) plotted on the same three principal component axes. Each point represents 55 seconds of activity between successive trials of the same odor within a block (solid circles) or successive one-minute bins of the intervals between blocks of different odors (open circles). **E.** K-NN classification based on angular distance of the glomerular response vectors during one-minute bins of the 15-minute IBI. The overall classification rate of the glomerular IBI activity was 34.8%.

References

1. Hildebrand, J. G. & Shepherd, G. M. Mechanisms of olfactory discrimination: converging evidence for common principles across phyla. *Annu. Rev. Neurosci.* **20**, 595–631 (1997).
2. Ache, B. W. & Young, J. M. Olfaction: diverse species, conserved principles. *Neuron* **48**, 417–430 (2005).
3. Buck, L. & Axel, R. A novel multigene family may encode odorant receptors: a molecular basis for odor recognition. *Cell* **65**, 175–187 (1991).
4. Sato, K. *et al.* Insect olfactory receptors are heteromeric ligand-gated ion channels. *Nature* **452**, 1002–1006 (2008).
5. Spors, H. & Grinvald, A. Spatio-temporal dynamics of odor representations in the mammalian olfactory bulb. *Neuron* **34**, 301–315 (2002).
6. Friedrich, R. W. & Laurent, G. Dynamic optimization of odor representations by slow temporal patterning of mitral cell activity. *Science* **291**, 889–894 (2001).
7. Szyszka, P., Gerkin, R. C., Galizia, C. G. & Smith, B. H. High-speed odor transduction and pulse tracking by insect olfactory receptor neurons. *Proc. Natl. Acad. Sci.* **111**, 16925–16930 (2014).
8. Masse, N. Y., Turner, G. C. & Jefferis, G. S. Olfactory information processing in Drosophila. *Curr. Biol.* **19**, R700–R713 (2009).
9. Jeanne, J. M. & Wilson, R. I. Convergence, divergence, and reconvergence in a feedforward network improves neural speed and accuracy. *Neuron* **88**, 1014–1026 (2015).
10. Olsen, S. R., Bhandawat, V. & Wilson, R. I. Divisive normalization in olfactory population codes. *Neuron* **66**, 287–299 (2010).

11. Zaborszky, L., Carlsen, J., Brashear, H. R. & Heimer, L. Cholinergic and GABAergic afferents to the olfactory bulb in the rat with special emphasis on the projection neurons in the nucleus of the horizontal limb of the diagonal band. *J. Comp. Neurol.* **243**, 488–509 (1986).
12. Cansler, H. L., Denson, H. B. & Wesson, D. W. Centrifugal innervation of the olfactory bulb: a reappraisal. *eNeuro* **6**, (2019).
13. Markopoulos, F., Rokni, D., Gire, D. H. & Murthy, V. N. Functional Properties of Cortical Feedback Projections to the Olfactory Bulb. *Neuron* **76**, 1175–1188 (2012).
14. Boyd, A. M., Sturgill, J. F., Poo, C. & Isaacson, J. S. Cortical Feedback Control of Olfactory Bulb Circuits. *Neuron* **76**, 1161–1174 (2012).
15. Linster, C., Henry, L., Kadohisa, M. & Wilson, D. A. Synaptic adaptation and odor-background segmentation. *Neurobiol. Learn. Mem.* **87**, 352–360 (2007).
16. Kay, L. M. & Laurent, G. Odor-and context-dependent modulation of mitral cell activity in behaving rats. *Nat. Neurosci.* **2**, 1003–1009 (1999).
17. Suh, E., Bohbot, J. D. & Zwiebel, L. J. Peripheral olfactory signaling in insects. *Curr. Opin. Insect Sci.* **6**, 86–92 (2014).
18. Imai, T., Sakano, H. & Vosshall, L. B. Topographic mapping—the olfactory system. *Cold Spring Harb. Perspect. Biol.* **2**, a001776 (2010).
19. Martelli, C., Carlson, J. R. & Emonet, T. Intensity invariant dynamics and odor-specific latencies in olfactory receptor neuron response. *J. Neurosci.* **33**, 6285–6297 (2013).
20. Arevian, A. C., Kapoor, V. & Urban, N. N. Activity-dependent gating of lateral inhibition in the mouse olfactory bulb. *Nat. Neurosci.* **11**, 80 (2008).
21. Sahay, A., Wilson, D. A. & Hen, R. Pattern separation: a common function for new neurons in hippocampus and olfactory bulb. *Neuron* **70**, 582–588 (2011).

22. Gschwend, O. *et al.* Neuronal pattern separation in the olfactory bulb improves odor discrimination learning. *Nat. Neurosci.* **18**, 1474–1482 (2015).

23. Thompson, P. & Burr, D. Visual aftereffects. *Curr. Biol.* **19**, R11–R14 (2009).

24. Patterson, M. A., Lagier, S. & Carleton, A. Odor representations in the olfactory bulb evolve after the first breath and persist as an odor afterimage. *Proc. Natl. Acad. Sci.* **110**, E3340–E3349 (2013).

25. Barlow, H. A theory about the functional role and synaptic mechanism of visual after-effects. *Vis. Coding Effic.* **363375**, (1990).

26. Kohn, A. Visual adaptation: physiology, mechanisms, and functional benefits. *J. Neurophysiol.* **97**, 3155–3164 (2007).

27. Saha, D. *et al.* Engaging and disengaging recurrent inhibition coincides with sensing and unsensing of a sensory stimulus. *Nat. Commun.* **8**, 1–19 (2017).

28. Sofroniew, N. J., Flickinger, D., King, J. & Svoboda, K. A large field of view two-photon mesoscope with subcellular resolution for in vivo imaging. *Elife* **5**, e14472 (2016).

29. Rinberg, D., Koulakov, A. & Gelperin, A. Speed-accuracy tradeoff in olfaction. *Neuron* **51**, 351–358 (2006).

30. Tichy, H. & Hellwig, M. Independent processing of increments and decrements in odorant concentration by ON and OFF olfactory receptor neurons. *J. Comp. Physiol. A* **204**, 873–891 (2018).

31. Virsu, V. & Laurinen, P. Long-lasting afterimages caused by neural adaptation. *Vision Res.* **17**, 853–860 (1977).

32. Vinograd, A., Livneh, Y. & Mizrahi, A. History-dependent odor processing in the mouse olfactory bulb. *J. Neurosci.* **37**, 12018–12030 (2017).

33. Whitmire, C. J. & Stanley, G. B. Rapid sensory adaptation redux: a circuit perspective. *Neuron* **92**, 298–315 (2016).

34. Huk, A. C., Ress, D. & Heeger, D. J. Neuronal Basis of the Motion Aftereffect Reconsidered. *Neuron* **32**, 161–172 (2001).

35. Mather, G., Pavan, A., Campana, G. & Casco, C. The motion aftereffect reloaded. *Trends Cogn. Sci.* **12**, 481–487 (2008).

36. Szyszka, P., Ditzen, M., Galkin, A., Galizia, C. G. & Menzel, R. Sparsening and temporal sharpening of olfactory representations in the honeybee mushroom bodies. *J. Neurophysiol.* **94**, 3303–3313 (2005).

37. Chalasani, S. H. *et al.* Dissecting a circuit for olfactory behaviour in Caenorhabditis elegans. *Nature* **450**, 63–70 (2007).

38. Nagel, K. I. & Wilson, R. I. Mechanisms underlying population response dynamics in inhibitory interneurons of the Drosophila antennal lobe. *J. Neurosci.* **36**, 4325–4338 (2016).

39. Nizampatnam, S., Zhang, L., Chandak, R., Li, J. & Raman, B. Invariant odor recognition with ON–OFF neural ensembles. *Proc. Natl. Acad. Sci.* **119**, e2023340118 (2022).

40. Chaudhury, D., Escanilla, O. & Linster, C. Bulbar acetylcholine enhances neural and perceptual odor discrimination. *J. Neurosci.* **29**, 52–60 (2009).

41. Burton, S. D. Inhibitory circuits of the mammalian main olfactory bulb. *J. Neurophysiol.* **118**, 2034–2051 (2017).

42. Chen, Z. & Padmanabhan, K. Top-down feedback enables flexible coding strategies in the olfactory cortex. *Cell Rep.* **38**, 110545 (2022).

43. Rothermel, M. & Wachowiak, M. Functional imaging of cortical feedback projections to the olfactory bulb. *Front. Neural Circuits* **8**, 73 (2014).

44. Böhm, E., Brunert, D. & Rothermel, M. Input dependent modulation of olfactory bulb activity by HDB GABAergic projections. *Sci. Rep.* **10**, 1–15 (2020).

45. Rothermel, M., Carey, R. M., Puche, A., Shipley, M. T. & Wachowiak, M. Cholinergic inputs from Basal forebrain add an excitatory bias to odor coding in the olfactory bulb. *J. Neurosci.* **34**, 4654–4664 (2014).

46. Chandak, R. & Raman, B. Neural manifolds for odor-driven innate and acquired appetitive preferences. *bioRxiv* 2021.08.05.455310 (2021) doi:10.1101/2021.08.05.455310.

47. Liu, G. *et al.* Target specific functions of EPL interneurons in olfactory circuits. *Nat. Commun.* **10**, 1–14 (2019).

48. Burton, S. D., Wipfel, M., Guo, M., Eiting, T. P. & Wachowiak, M. A novel olfactometer for efficient and flexible odorant delivery. *Chem. Senses* **44**, 173–188 (2019).

49. Saha, D. *et al.* A spatiotemporal coding mechanism for background-invariant odor recognition. *Nat. Neurosci.* **16**, 1830–1839 (2013).

50. Pouzat, C., Mazor, O. & Laurent, G. Using noise signature to optimize spike-sorting and to assess neuronal classification quality. *J. Neurosci. Methods* **122**, 43–57 (2002).

51. Saha, D. *et al.* Behavioural correlates of combinatorial versus temporal features of odour codes. *Nat. Commun.* **6**, 6953 (2015).

52. Nizampatnam, S., Saha, D., Chandak, R. & Raman, B. Dynamic contrast enhancement and flexible odor codes. *Nat. Commun.* **9**, 3062 (2018).

Figure 1: Odor ON and OFF responses in the locust antenna lobe are anticorrelated

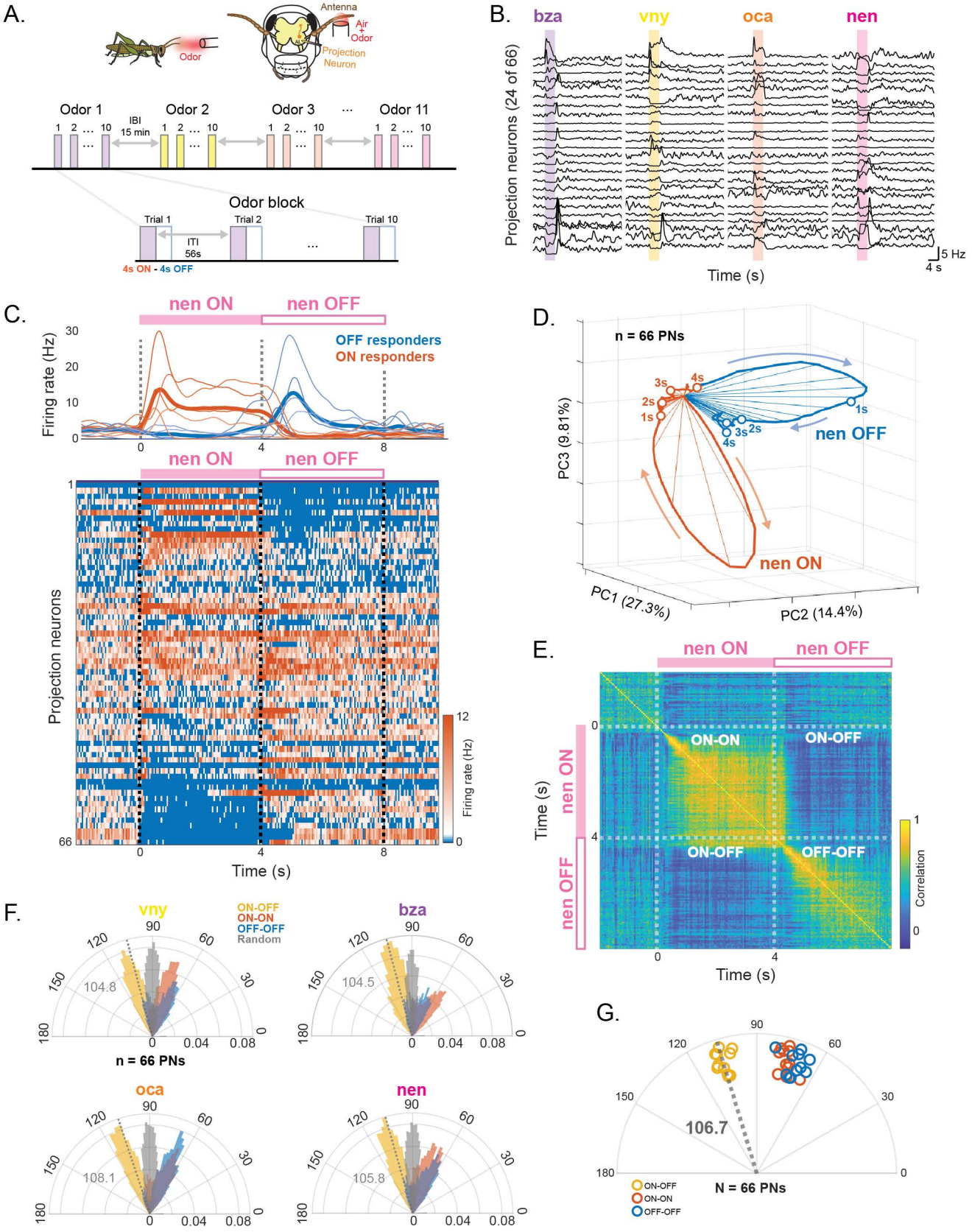

Figure 2: Odor ON and OFF responses in the mouse olfactory bulb are anticorrelated

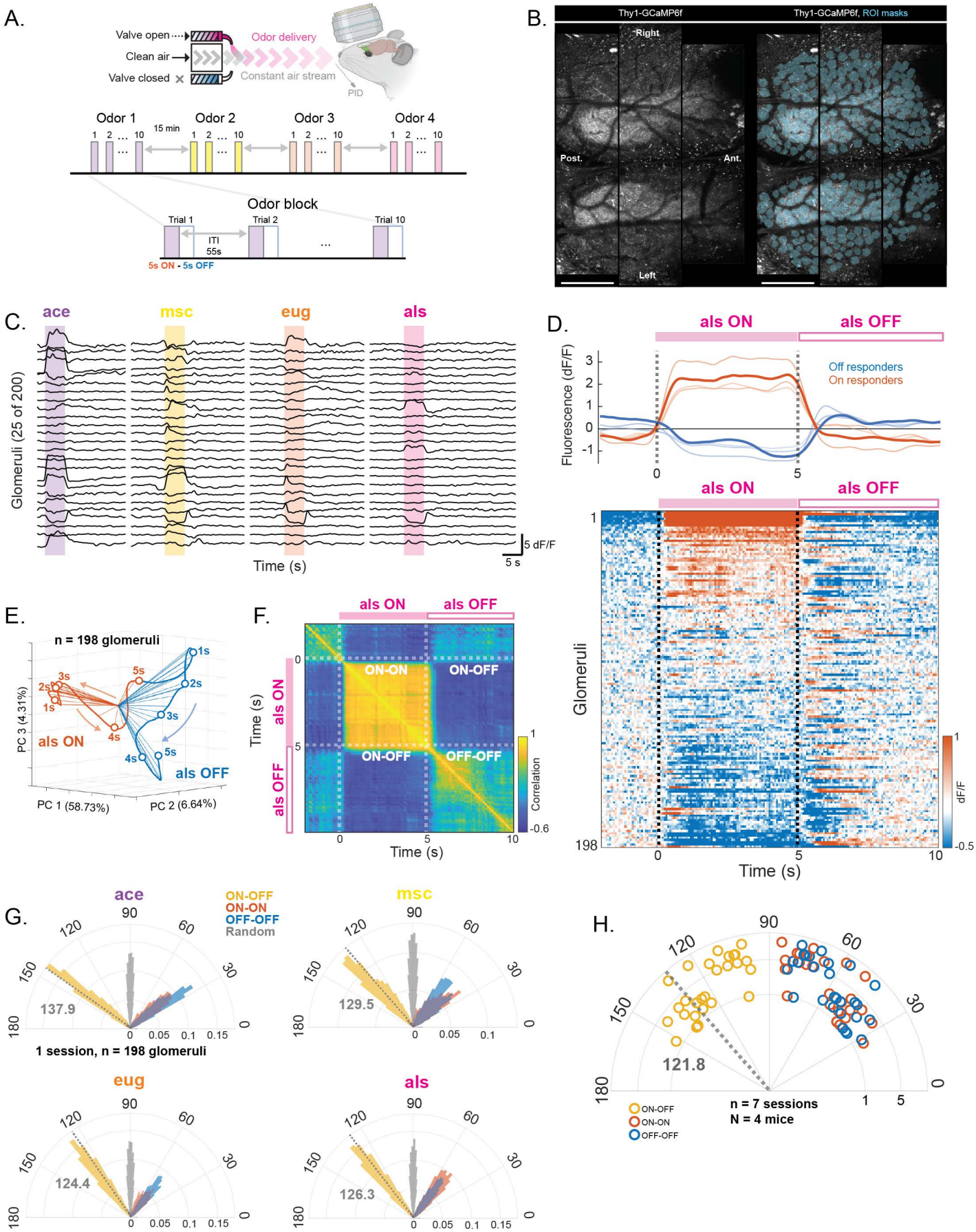

Figure 3: ON and OFF responses in locust antenna lobe contain distinct odor specific information

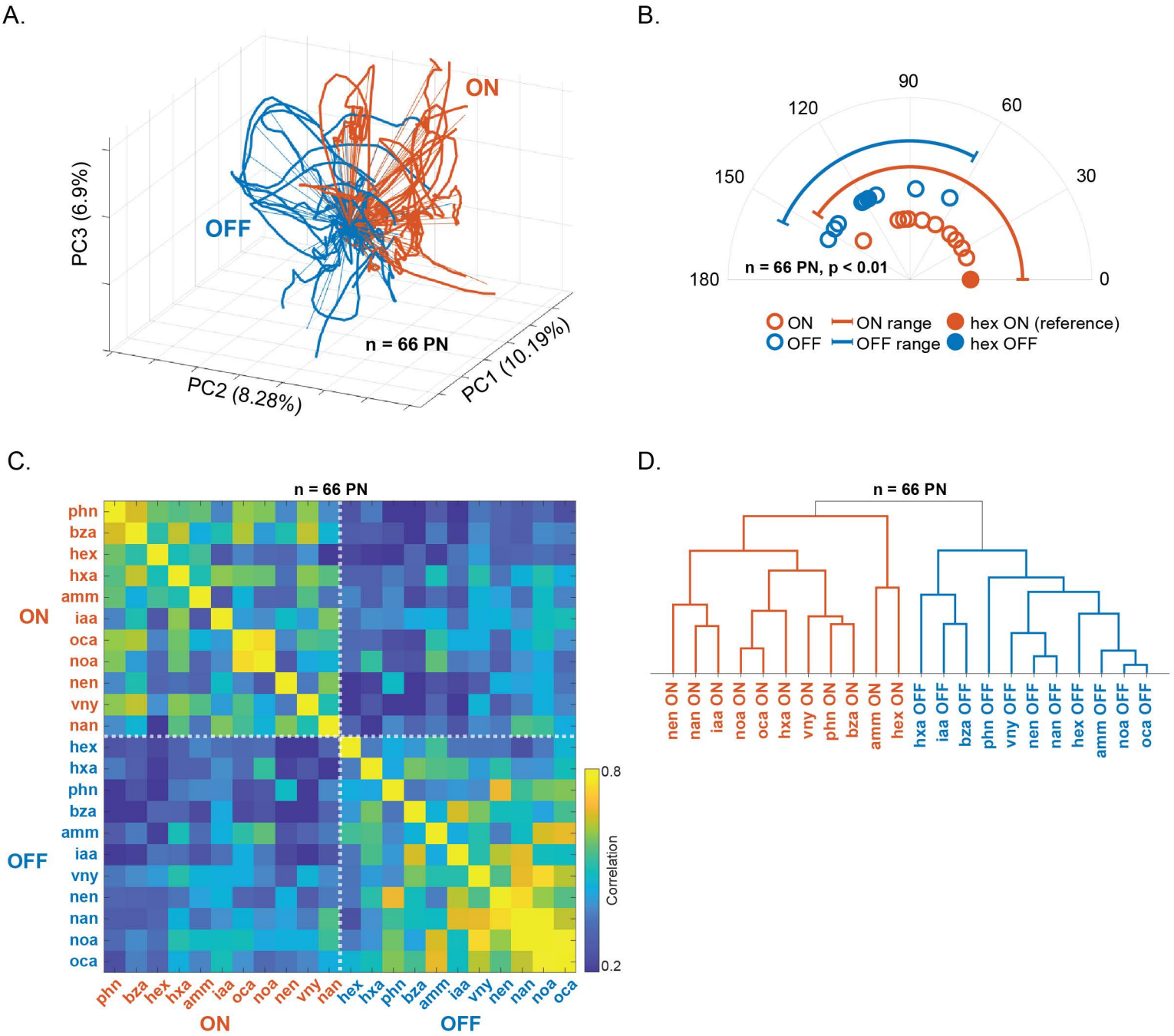

Figure 4: Odor ON and OFF responses in the mouse olfactory bulb contain distinct odor specific information

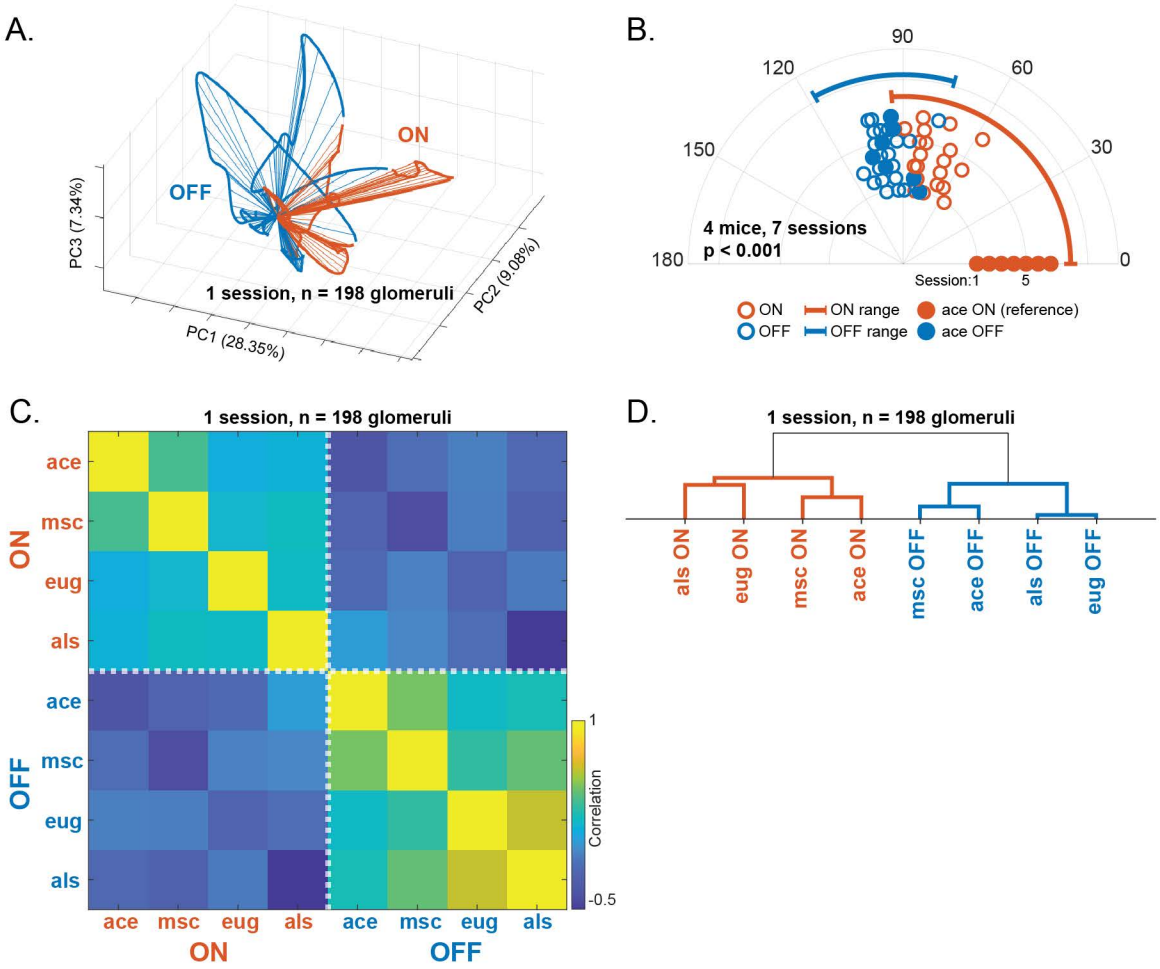

Figure 5: Contrast between sequential odors is enhanced in the locust antenna lobe

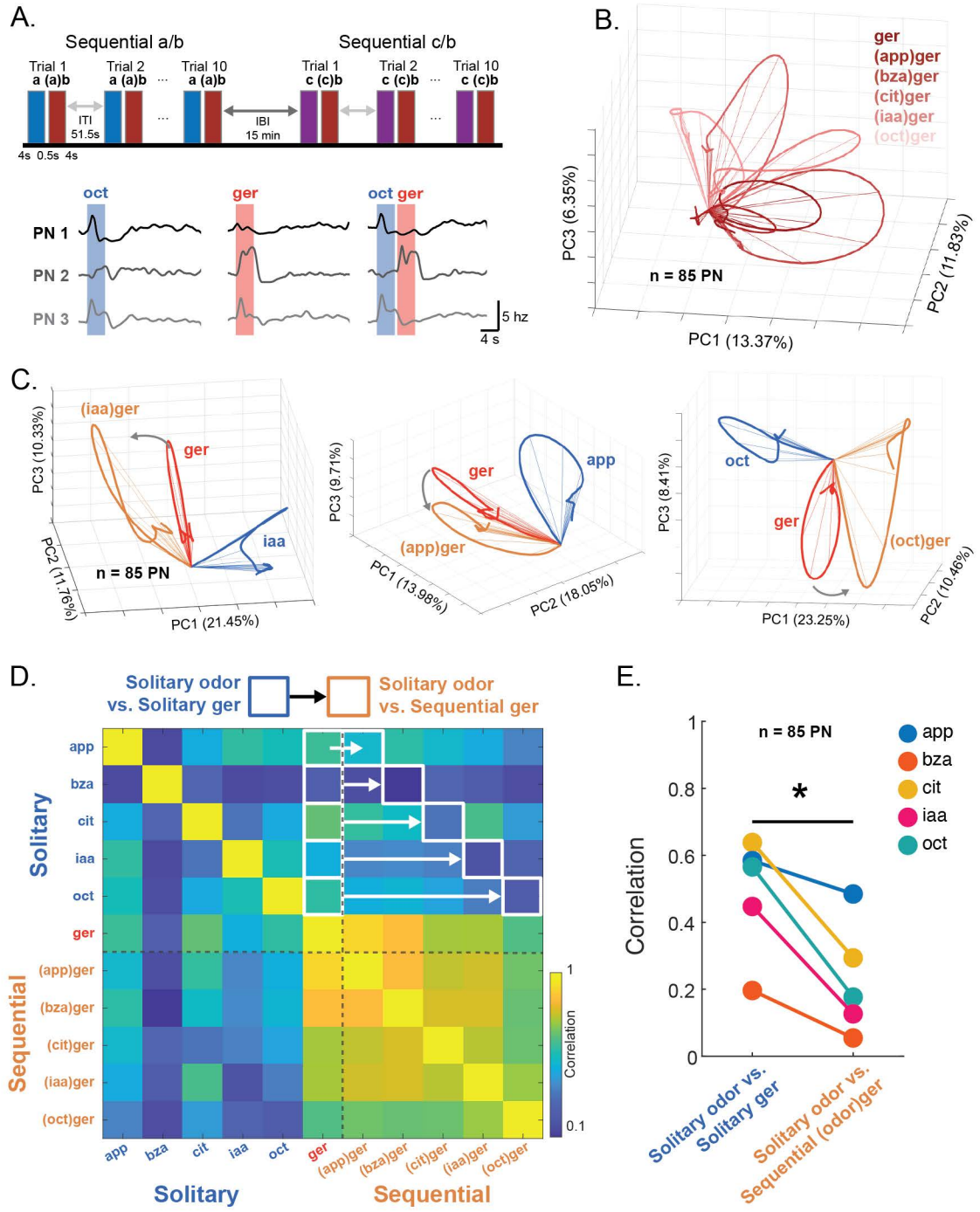

Figure 6: Contrast between sequential odors is enhanced in the mouse olfactory bulb

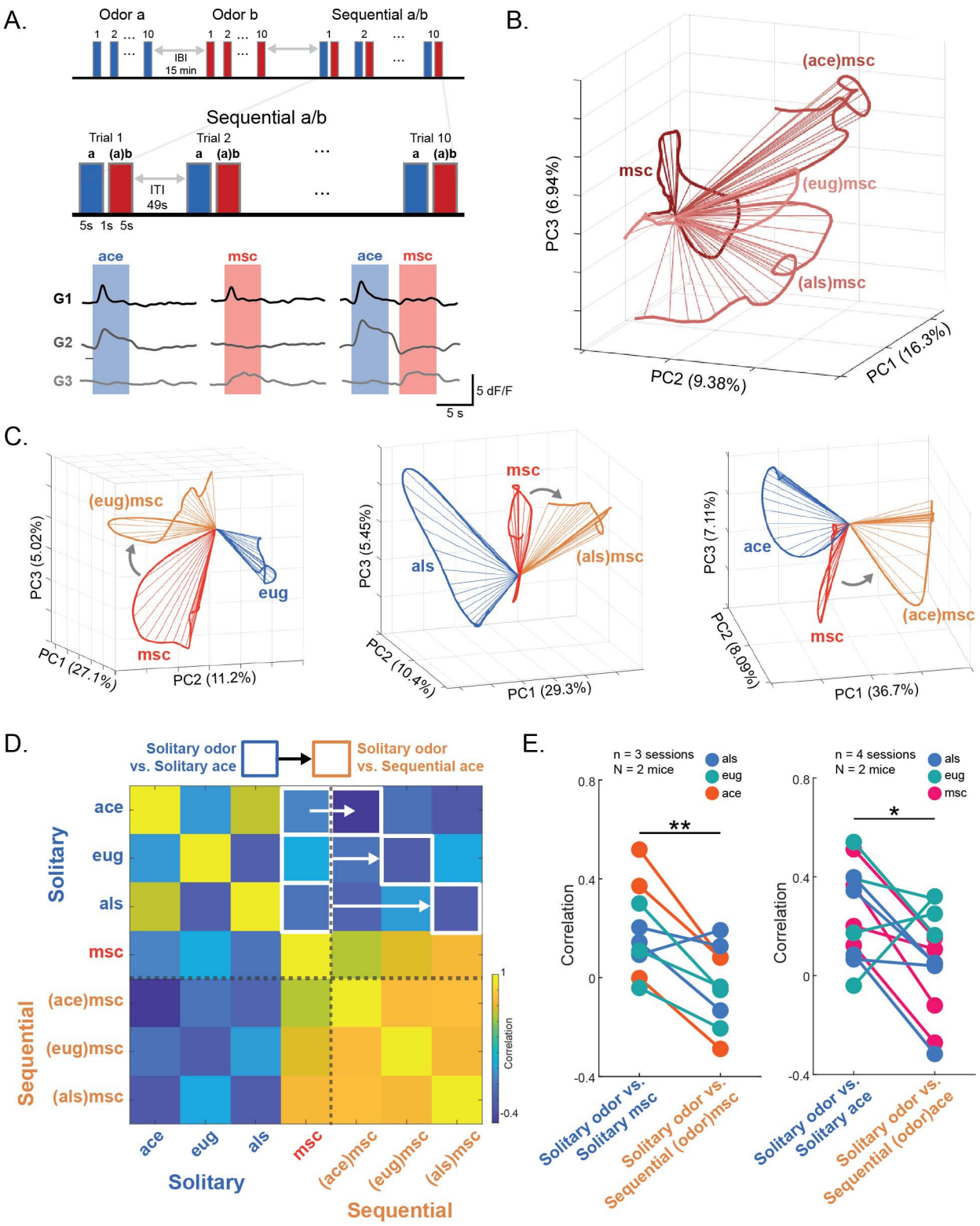

Figure 7: OFF responses maintain an odor-specific short term memory in mouse OB and locust AL

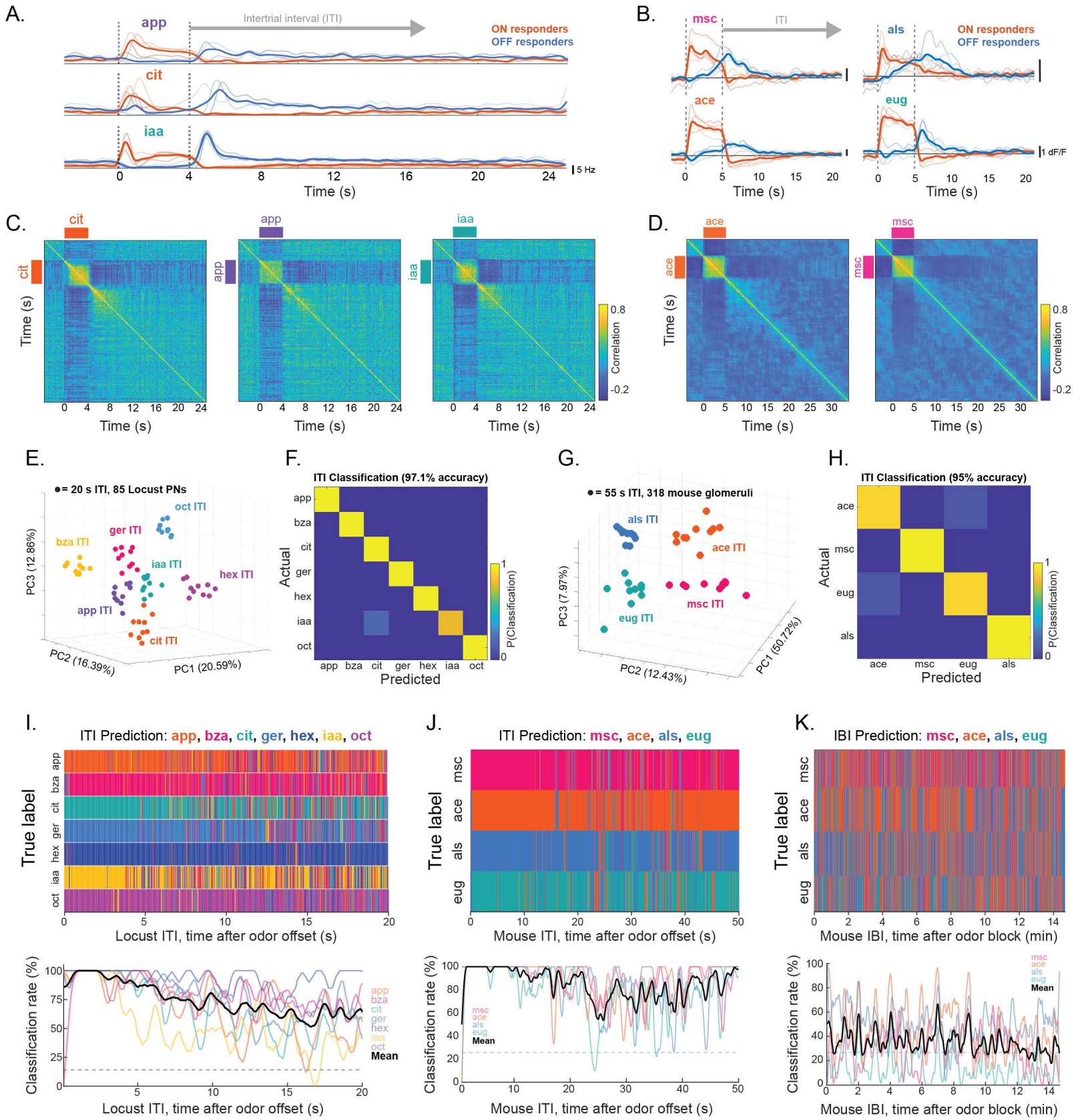

Figure S1: angle distributions for the other odors

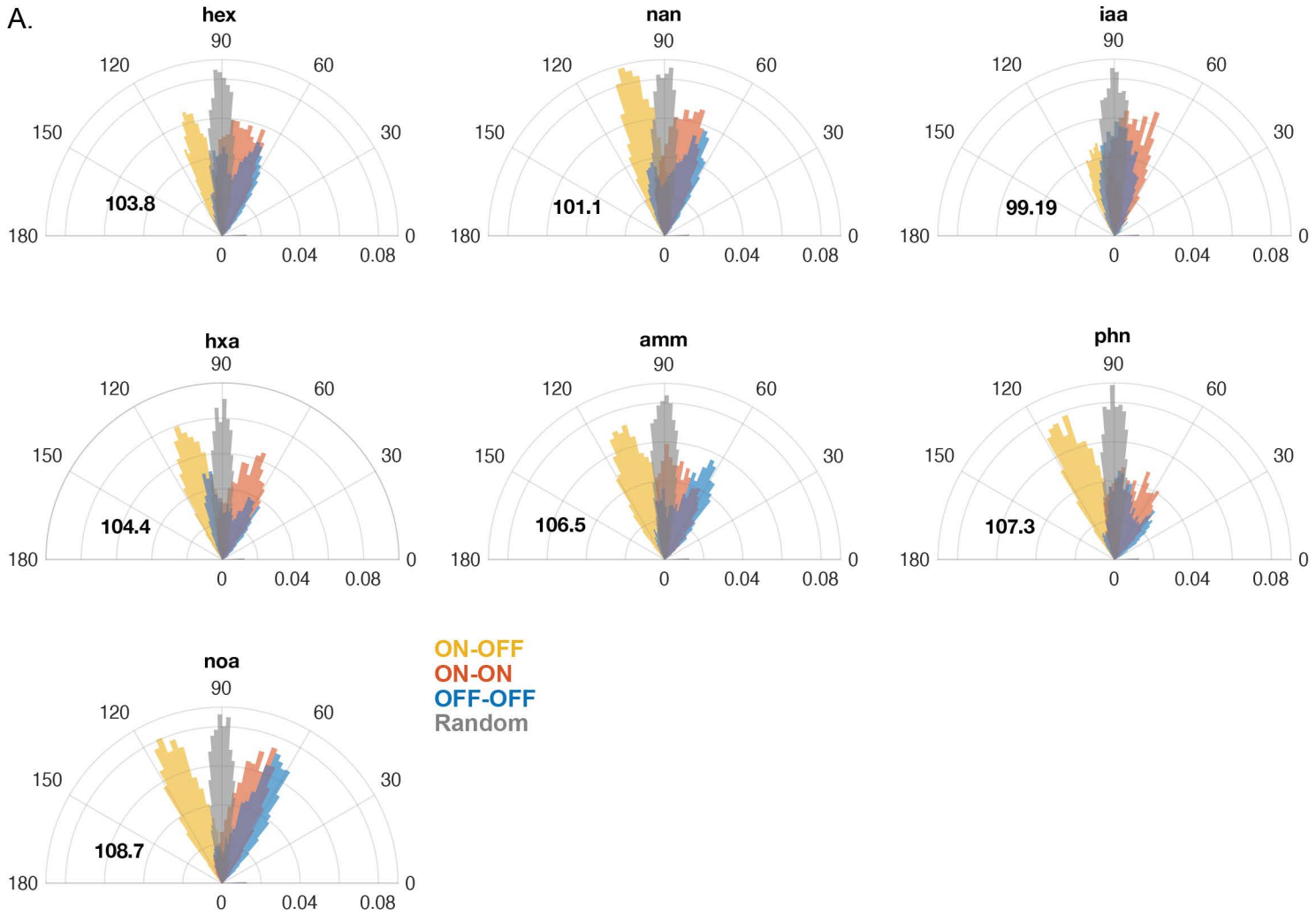

Figure S2: separate ON and OFF PCA

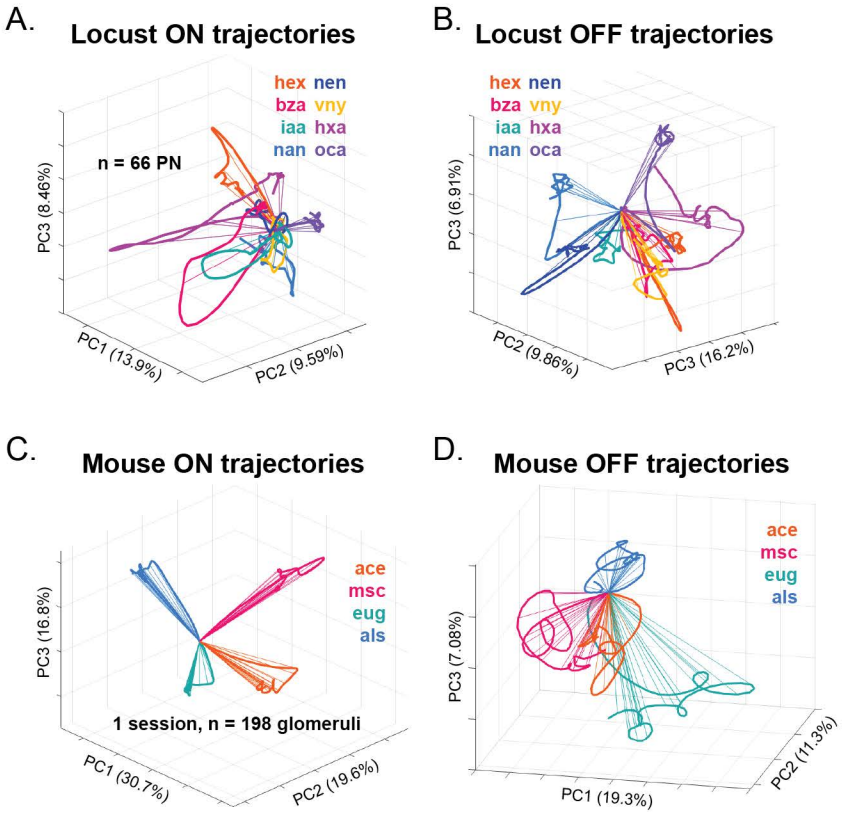

Figure S3: ON vs OFF angles with different reference odors (mouse and locust)

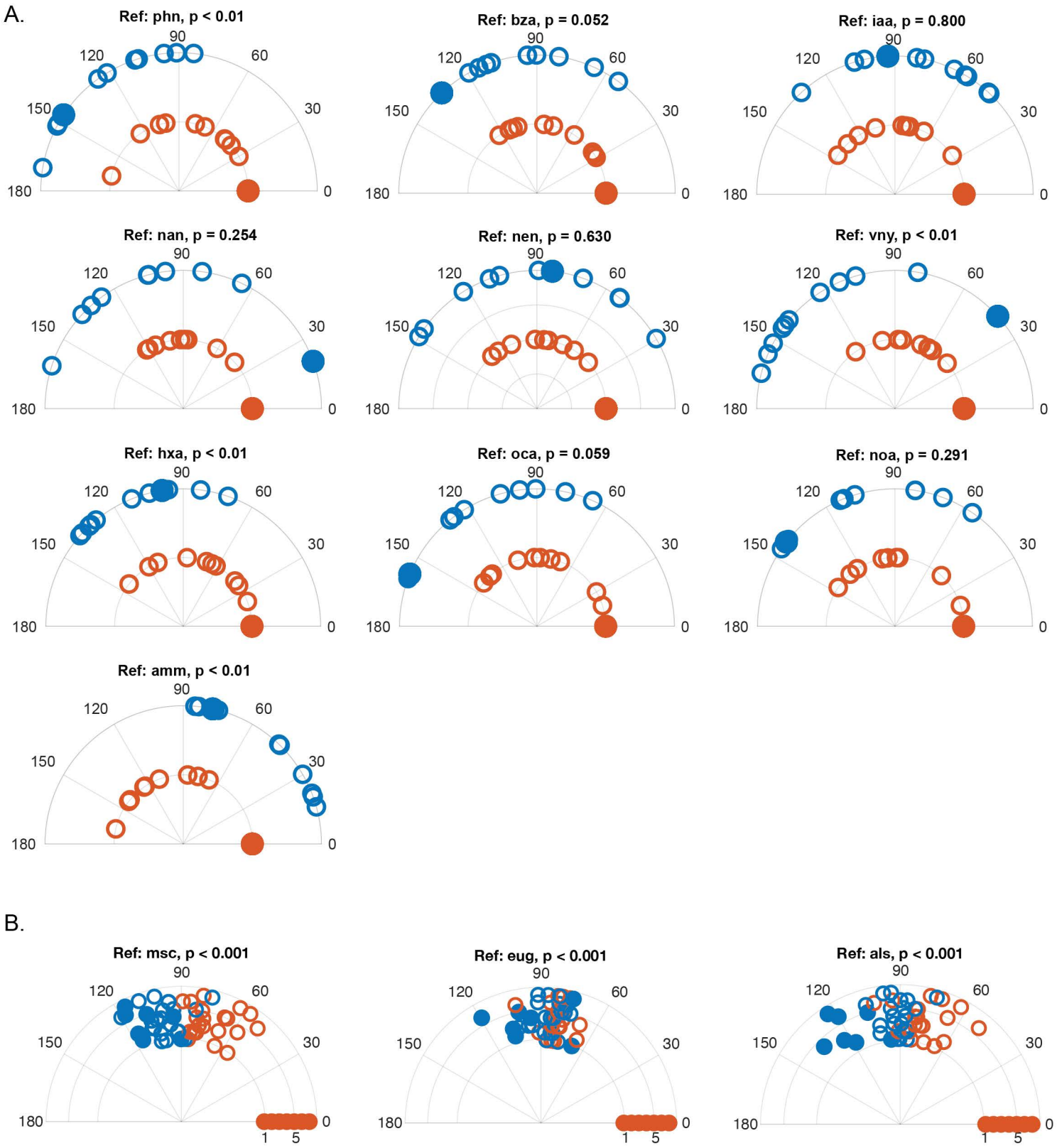

Figure S4: Distributions of correlation values for inter and intra-period correlations in mouse and locust

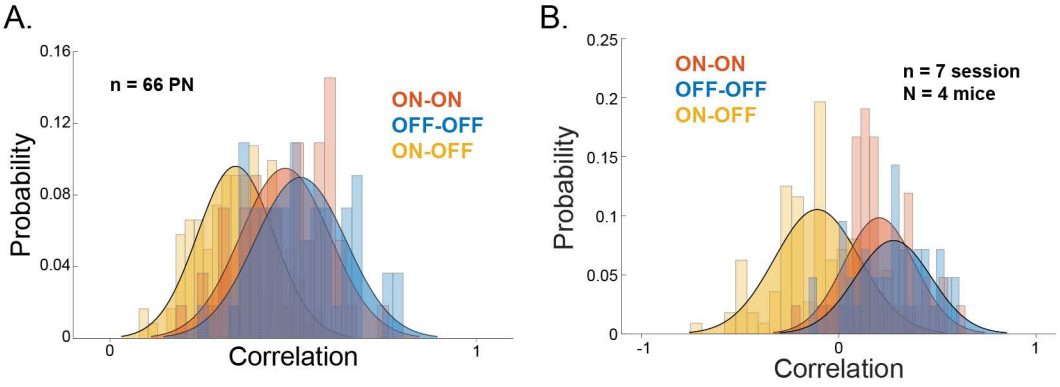

Figure S5: Contrast enhancement in the mouse olfactory bulb generalizes across odors.

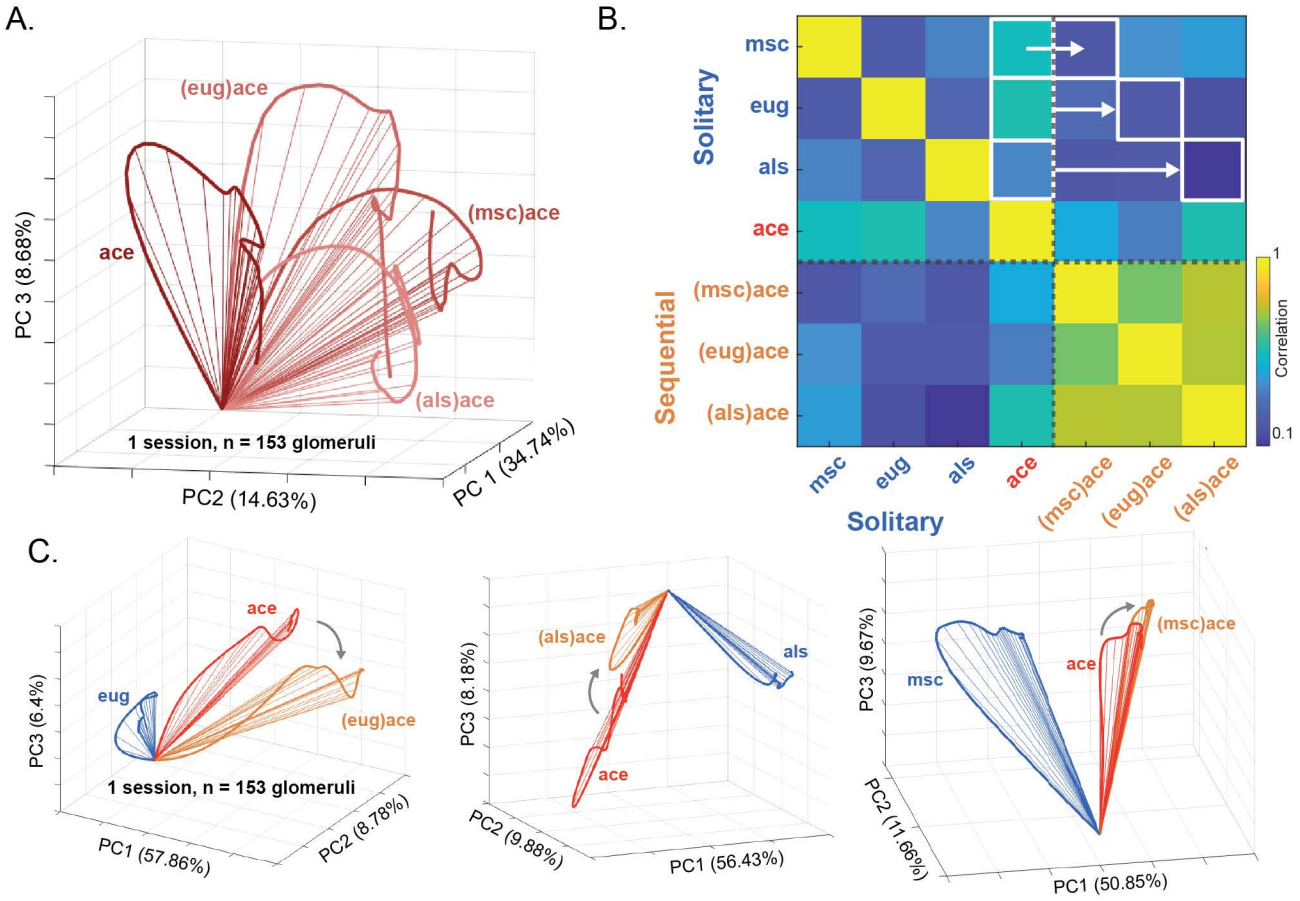

Figure S6: OFF response persistence across odors through the ITI and IBI

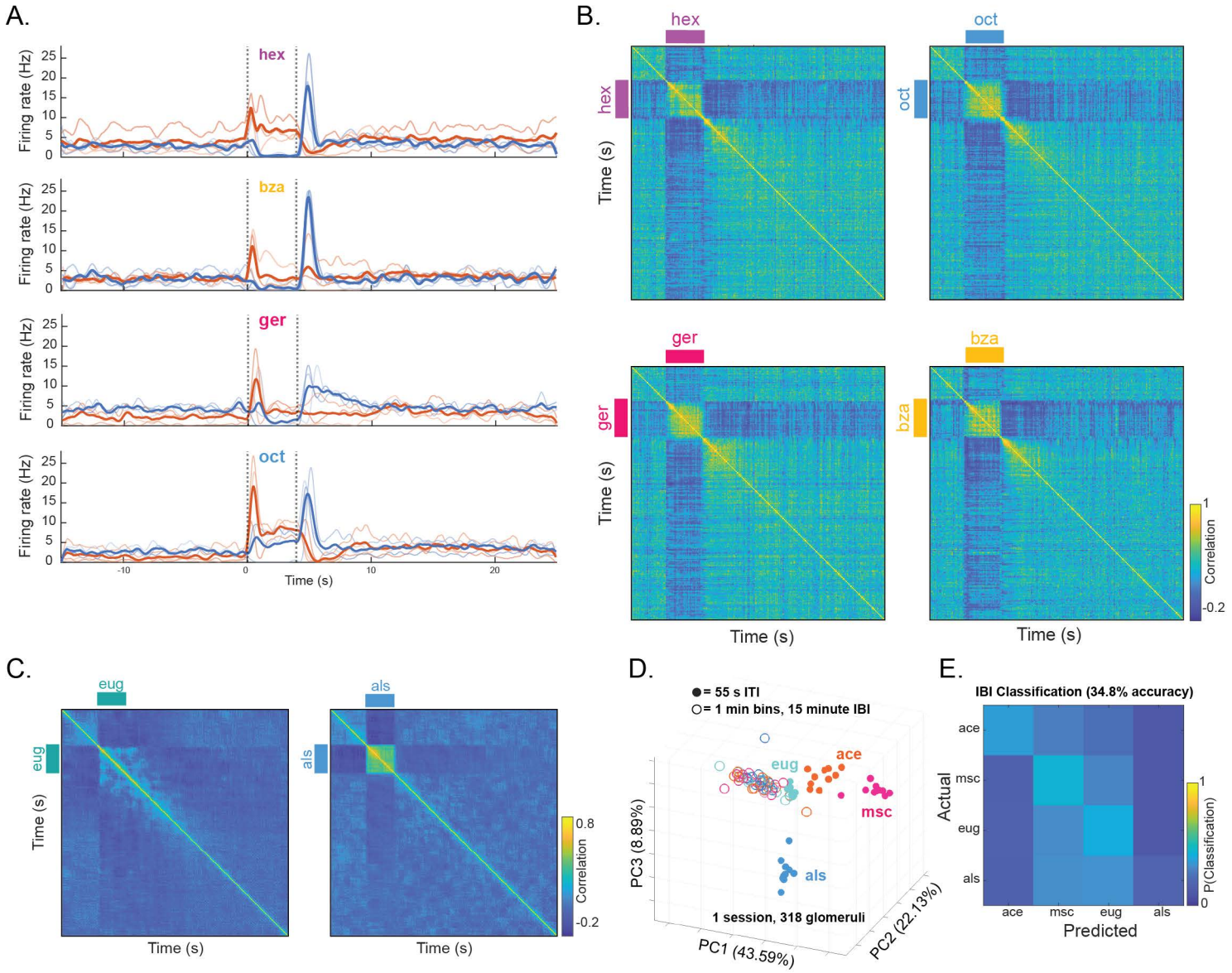

Figure	Dataset(s)
1	Locust dataset 1: 66PNs across 15 animals
2c-g	Mouse 2, session 3: 198 glomeruli
2h	7 Mouse datasets: m1, session 1, 73 glomeruli; m2, session1, 210 glomeruli; m2 session 2, 153 glomeruli; m2, session 3, 198 glomeruli; m3, session 1, 286 glomeruli; m4, session 1, 219 glomeruli; m4, session 2, 318 glomeruli
3	Locust dataset: 66PNs across 15 animals
4	Mouse 2, session 3: 198 glomeruli
5	Reanalysis of locust dataset from[52]: 85PNs across 9 animals
6a-d	Mouse 4, session 1: 219 glomeruli
6e, left	3 Mouse datasets: m3, session 1; m4, session 1; m4, session 2
6e, right	4 Mouse datasets: m1, session 1; m2, session 1; m2, session 2; m2, session 3
7a, c, e, f, i	Reanalysis of locust dataset from[52]: 85PNs across 9 animals
7b,d,g,h,j,k	Mouse 4, session 2: 318 glomeruli
S1	Locust dataset 1: 66PNs across 15 animals
S2a, b	Locust dataset 1: 66PNs across 15 animals
S2c, d	Mouse 2, session 3: 198 glomeruli
S3a	Locust dataset #1: 66PNs across 15 animals
S3b	7 mouse datasets: m1, session 1; m2, session 1; m2, session 2; m2, session 3; m3, session 1; m4, session 1; m4, session 2
S4a	Locust dataset #2: 85PNs across 9 animals
S4b	Mouse 2, session 3: 198 glomeruli
S5	Mouse 2, session 2: 153 glomeruli
S6a-b	Reanalysis of locust dataset from[52]: 85PNs across 9 animals
S6c-d	Mouse 4, session 2: 318 glomeruli

Table 1. Datasets analyzed and/or displayed for each figure.